An *In Vitro* Flow System to Study the Endothelial Cell Response to Positive and Negative Wall Shear Stress Gradients

By

Sukhjinder Singh

August 21st, 2009

A thesis submitted to the Faculty of the Graduate School of the

State University of New York at Buffalo in partial fulfillment of the requirements for the

degree of

Master of Science

Department of Mechanical and Aerospace Engineering

ACKNOWLEDGEMENT

It is a pleasure to thank the many people who made this thesis possible.

It is difficult to overstate my gratitude to my advisor, Dr. Hui Meng. With her enthusiasm, her inspiration, and her great efforts to explain things clearly and simply, she helped to make this project a great learning experience. Throughout this work, she provided encouragement, sound advice, good teaching, good company, and lots of good ideas.

Special thanks are due to my co-advisor Dr. John Kolega, for taking intense academic interest in this study as well as providing valuable suggestions that improved the quality of this study. His knowledge and experience in cell biology and *in vitro* experiments, significantly helped my work.

I also wish to express my appreciation to Dr. Rober Baier, on behalf of devoting his precious time and making many valuable suggestions which indeed helped improve of this thesis. I thank him for reviewing my work and enriching the discussions with critical questions. His passionate approach for explaining ideas, helped me learn a lot in a very short duration.

I am very grateful to Dr. Markus Tremmel for his guidance and insight for my CFD calculations. I am also thankful to Scott Woodward for his support in manufacturing the chamber and solving technical problems related to its working.

I am also very thankful to fellow graduate student Jennifer Dolan who introduced me to *in vitro* studies. Without her perseverance and hard work for in vitro experiments, this thesis would not have been possible.

Many thanks to my friends and colleagues at TSRC (Toshiba Stroke Research Center) for making it an amusing experience: Ding Ma, Jianping Xiang, Eleni Metaxa, Ling Gao, Max Mandelbaum and Nicholas Liaw.

Finally, I would like to express my sincere gratitude to my father for his love and support throughout my education. I thank him for being a true inspiration in my life.

TABLE OF CONTENTS

ACKNOWLEDGEMENTS. iii

LIST OF FIGURES vii

ABSTRACT x

CHAPTER 1: INTRODUCTION 1

1.1 Intracranial Aneurysms 1

1.2 Importance of Hemodynamics in Aneurysm Initiation 3

1.3 Endothelium and Abnormal Hemodynamics 4

1.4 *In Vitro* studies of Endothelium Response to Flow 6

1.5 Objectives 7

CHAPTER 2: DESIGN OF *IN* VITRO FLOW SYSTEM 8

2.1 Objectives 8

2.2 Study of Existing Flow Systems 9

2.2.1 Parallel plate flow system 9

2.2.2 Cone and plate flow system 10

2.2.3 Step Chamber 11

2.2.4 Radial flow chamber 12

2.2.5 Stagnation point flow chamber 12

2.2.6 Capillary perfusion chamber 13

2.3 Determination of Values of Shear Stress and Gradients to be Studied 13

2.4 Theoretical Flow Chamber Design 14

2.5 Application of CFD to Optimize Conditions 18

2.6 CFD Results 22

2.7 Joining the Chambers in Series 25

2.8 Flow Chamber Manufacturing 26

2.9 Flow Loop Design 27

CHAPTER 3: DESCRIPTION OF BIOLOGICAL ASSAYS FOR THE *IN VITRO* STUDIES

3.1 Cell Culture 30

3.2 Experimental Protocol 30

3.3 Morphological Examination 32

CHAPTER 4: EXPERIMENTAL RESULTS OF *IN VITRO* STUDIES 33

4.1 Cell Morphology and Alignment 33

CHAPTER 5: CONCLUSIONS AND FUTURE STUDIES 43

APPENDIX A: FLOW CHAMBER DEVELOPMENT 45

APPENDIX B: NOTES ON *IN VITRO* FLOW LOOP DEVELOPMENT 53

APPENDIX C: *IN VITRO* RESULTS 60

REFERENCES 68

List of Figures

Figure 1. Intracranial aneurysms. 11

Figure 2. Common Sites of Intracranial Aneurysms on the Circle of Willis. 12

Figure 3. Location of endothelial cells in blood vessels. 14

Figure 4. Endothelial cells and hemodynamic forces. 15

Figure 5. Parallel Plate Flow Chamber. 20

Figure 6. Cone and Plate viscometer. 21

Figure 7. Step Chamber.....22

Figure 8. Radial Flow System. 22

Figure 9. Theoretical design of chamber. 27

Figure 10. Intial 3D model designed in Pro Engineer. 28

Figure 11. Meshed 3D model, mesh generated in ICEM-CFD. 29

Figure 12. Side view of the mesh shows how mesh density increases in thinner sections. 30

Figure 13. WSS contours on the chamber surface. 32

Figure 14. WSS contour along the chamber base. 32

Figure 15. WSS and WSSG variation on the chamber base (converging section). 33

Figure 16. WSS and WSSG variation on the chamber base (diverging section). 33

Figure 17. Streamlines in the diverging section. 34

Figure 18. Final model of chamber with two converging and two diverging sections. Designed in Pro Engineer. 35

Figure 19. Placement of endothelial cell in the flow chamber and flow exposure. 36

Figure 20. Flow chamber secured with polycarbonate plates and screws. (Pro Engineer). 37

Figure 21. Flow Loop Design. 38

Figure 22. Experimental Protocol. 41

Figure 23. Illustration of measurement of alignment, θ and elongation, a. 43

Figure 24. Cell morphology showing fitted ellipses and polar plots for baseline WSS and positive WSSG. 46

Figure 25. Cell morphology showing fitted ellipses and polar plots for high WSS and negative WSSG. 49

Figure 26. Comparison of positive and negative WSSG regions in same WSS range. ……50

Figure 27. Student T test Results. …….52

Figure 28. Top view of the chamber, which was designed using Pro Engineer. Dimensions are expressed in inches. 55

Figure 29. Front view of chamber, which was designed using Pro Engineer. Dimensions are expressed in inches. 55

Figure 30. The design was split into two halves, the upper and lower and both halves were manufactured by CNC machining. 56

Figure 31. Top view of the mould used for upper section, designed in Pro Engineer. Dimensions are expressed in inches. 57

Figure 32. Top view of the mould used for the lower section. Designed in Pro Engineer. Dimensions are expressed in inches. 57

Figure 33. Polycarbonate plates that were used to seal the two silicone parts. Designed in Pro Engineer. Dimensions expressed in inches. 58

Figure 34. Connector, designed to connect the chamber to tubing. Designed in Pro Engineer. ..59

Figure 35. A) Molds used for the upper and lower section of designed chamber. B) Final chamber after the cured silicone elastomer was removed from molds. ……60

Figure 36. Reynolds number in the converging section. 62

Abstract

The apparent tendency of intracranial aneurysms to form at apices of cerebral bifurcations and outer sides of curved vessels, has led to many speculations that high wall shear stress (WSS) damages the arterial wall, starting from the inner layer: the endothelial cells (ECs). However, little is known about EC response to high WSS and wall shear stress gradients (WSSG). In this study the influence of WSS and WSSG on endothelial cell biology was examined under the hypothesis that initiation of intracranial aneurysms involves a local functional alteration in endothelium mediated by fluid shear stress and shear stress gradients. For this purpose, a flow chamber with converging and diverging sections was designed to expose cultured bovine aortic endothelial cells to positive and negative WSSGs. The chamber was designed such that effects of gradients at constant magnitude could be studied and simultaneously compared with zero gradient regions. The flow experiments ran for 24 hours. Endothelial cell morphology was investigated in relation to local flow characteristics and shear stress forces. Individual cell morphology and cell shape distribution in the monolayers were assessed using a computerized image analysis system. When exposed to wall shear stress gradients, cultured endothelial cells exhibited a dramatic response to characteristics of the flow. It was found that cells respond differently to negative and positive gradients. While in positive WSSG regions ECs aligned away from the flow, they were very well aligned with the flow in negative WSSG regions of nearly same magnitude. ECs were also found aligned with the flow in low WSS regions but were almost aligned perpendicular to the flow in high WSS regions. This investigation is one of the first to qualitatively compare effects of positive and negative WSSGs on vascular endothelial cells.

CHAPTER 1

INTRODUCTION

Since the motivation for this study originated from the intracranial aneurysm (IA) pathology, a description of this vascular disease will first be presented.

1.1 Intracranial Aneurysms

An aneurysm is widening or bubble in the wall of a blood vessel. When such a bubble appears in the head, it is called an "intracranial aneurysm." These aneurysms are extraordinarily dangerous because they can burst, flooding the brain or skull with blood. This condition is called a *subarachnoid hemorrhage*. A subarachnoid hemorrhage causes tremendous pressure inside the skull, often with devastating effect. Approximately 12 percent of patients die before receiving medical attention,[1] 40 percent of hospitalized patients die within one month after the event, and more than one third of those who survive have major neurologic deficits.[2-6] If left untreated, other outcomes include persistent confusion or stupor and coma.

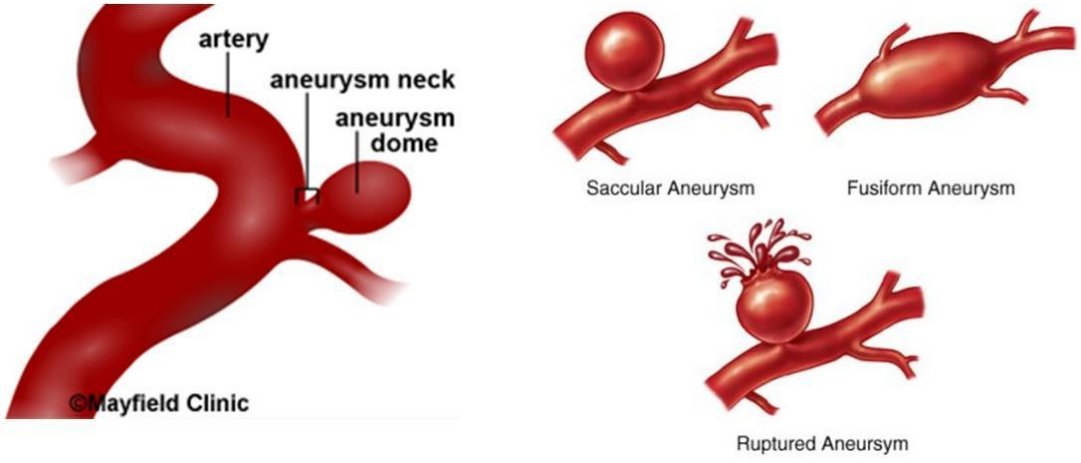

Figure 1. Intracranial aneurysms (Image from mayfieldclinic.com)

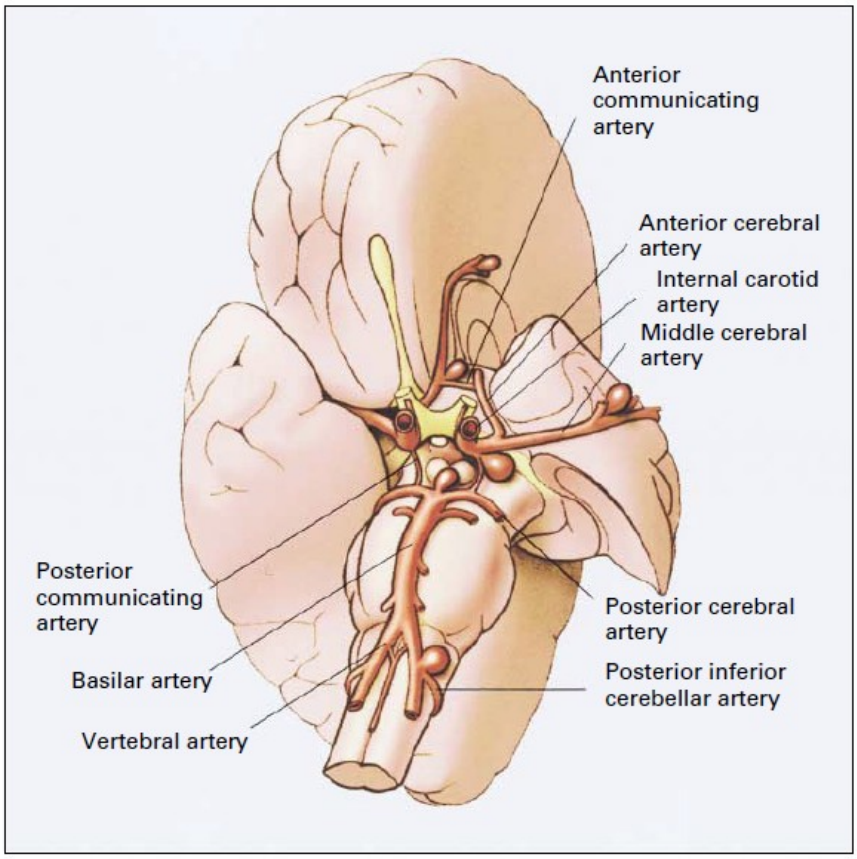

Figure 2. Common Sites of Intracranial Aneurysms on the Circle of Willis. [1]

Intracranial aneurysms are common, with a prevalence of 0.5% to 6% in adults, according to angiography and autopsy studies.[7] Most intracranial aneurysms are asymptomatic and are never detected. Some are discovered incidentally in neuroimaging studies and some produce symptoms due to compression of neighboring nerves or adjacent brain tissue. Others are detected only after they have ruptured and caused subarachnoid hemorrhage, with 32% to 67% case fatality and 10% to 20% long-term dependence in survivors due to brain damage.[8]

Aneurysms may result from congenital defects, preexisting conditions such as high blood pressure and atherosclerosis (the buildup of fatty deposits in the arteries), or head trauma.

Cerebral aneurysms occur more commonly in adults than in children but they may occur at any age. They are more common in women than in men, by a ratio of 2 to 1.[9]

Little is known about their initiation and growth, and rupture has proven highly unpredictable.[10, 11] As a result, treatment decisions are difficult to make and even treated aneurysms are associated with high morbidity and mortality.[12, 13]

1.2 Importance of Hemodynamics in Aneurysm Initiation

Although the exact mechanism of aneurysm initiation is not known, previous work has shown that hemodynamics plays a critical role in the initiation of intracranial aneurysms.[14, 15] It was found that high WSS and very high WSSGs correspond to loss of the internal elastic lamina, a thinned media, loss of smooth muscle cells, and degradation of the matrix, all of which are characteristics of early aneurysms. Most intracranial aneurysms occur at or near arterial bifurcations.[16, 17] High WSS and high WSSGs (positive and negative) are characteristic of hemodynamic environments near bifurcations.

The arterial circulation is a complex system where non-Newtonian, pulsatile, compliant and geometrical effects need to be considered to describe in detail flow dynamics and force magnitudes acting on the arterial wall.

A plethora of research has been done to precisely define the nature of disturbed flow patterns associated with different arterial diseases. Various methodologies have been employed for this purpose including working with post mortem human arteries made transparent by oil treatment[18] and constructing vascular casts and transparent models.[19-22] With the development of supercomputers and advanced numerical codes, full numerical simulations of the

problems which involve non-Newtonian, pulsatile, compliant and geometrical effects have become available.[23-25]

The regions of arterial branching and sharp curves are favored sites for development of various diseases. In an arterial bifurcation, the inner wall adjacent to the flow divider which has greatest predilection for aneurysm initiation, is exposed to unidirectional laminar flow with strong variation in wall shear stress and shear stress gradients. The perturbed flow region is localized on the outer wall, opposite to the flow divider which correlates well with the location of atherosclerosis.[22, 26]

1.3 Endothelium and Abnormal Hemodynamics

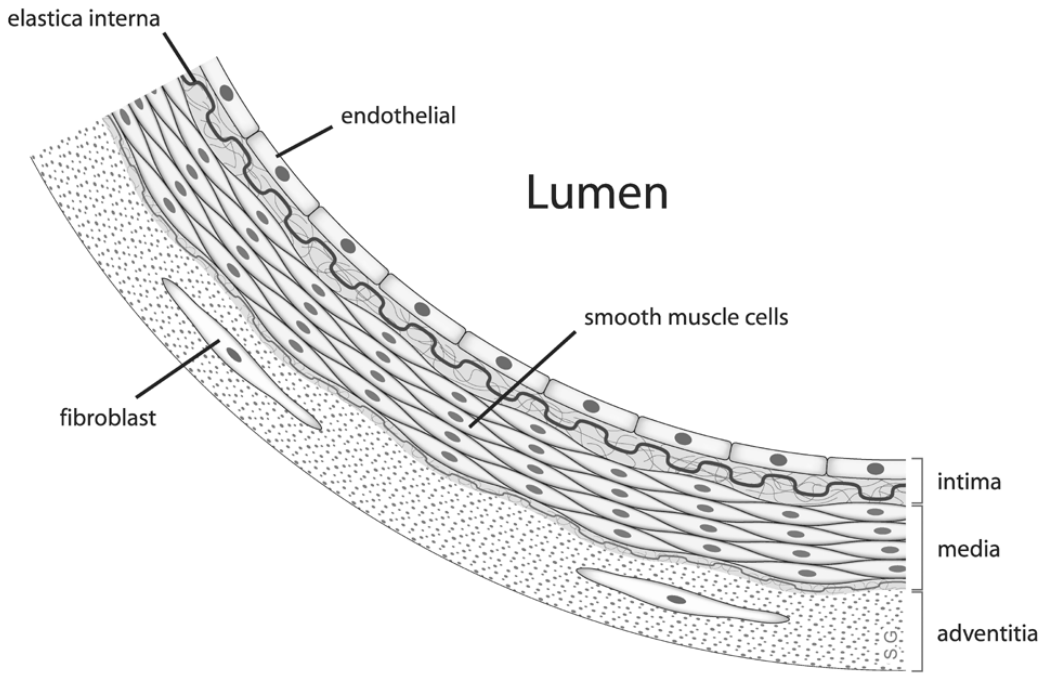

Figure 3. Location of endothelial cells in blood vessels

Endothelium is thin layer of flattened cells that line the interior surface of blood vessels, forming an interface between circulating blood in the lumen and the rest of the vessel wall. Damage and alteration of endothelium has been implicated in the pathophysiology of arterial diseases. The response of endothelium to shear stress and shear stress gradients is not completely known, and a purpose of this research is to study this response.

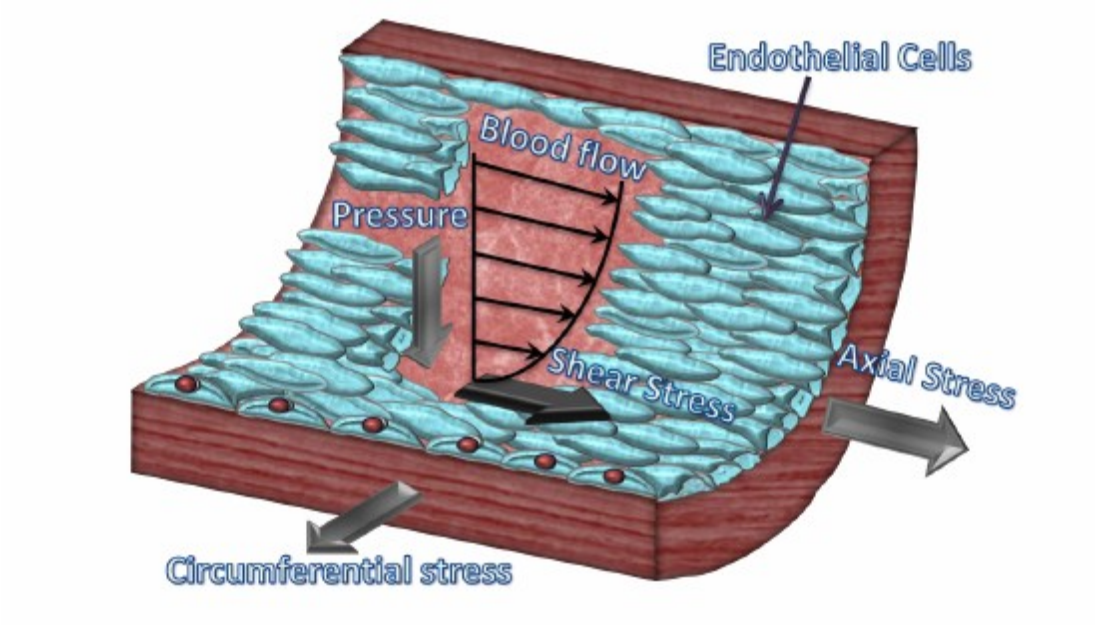

Figure 4. Endothelium and hemodynamic forces

The endothelium, by virtue of its unique location in the vessel wall, responds rapidly and sensitively to the mechanical conditions created by blood flow and the cardiac cycle. As a result of their unique location, endothelial cells experience three primary mechanical forces: a) pressure, which acts perpendicular to the surface and it is transmitted to the elastic subendothelial structures; b) shear stress, which is resisted by the endothelial cells themselves; and c) circumferential stretch or tension, created as a result of defined intercellular connections

between the endothelial cells that exert longitudinal forces on the cell during vasomotion. Of these forces, shear stress appears to be a particularly important hemodynamic force because it stimulates the release of vasoactive substances and changes gene expression, cell metabolism, and cell morphology.[27] Acute and chronic control of lumen diameter in response to changing flow is endothelium dependent, thus establishing its role as a mechanotransducer for the blood vessel.[28, 29] The alignment of endothelial cells in response to flow is among the earliest evidence of mechanotransduction in the endothelium. [30] Measures of the two-dimensional shape change of the cells were used to quantify the response.[31]

1.4 *In Vitro* Studies of Endothelium Response to Flow

In the last three decades, the in vitro morphological and functional responses of endothelial cells to shear stresses in laminar and turbulent flows have been widely investigated. Shear stress has been found to have a significant effect on endothelial cell morphology, cytoskeleton organization, membrane mechanical properties, intracellular signaling, endocytosis, cell cycle entry, activation of ion channels, messenger RNA, protein synthesis, LDL metabolism and mobilization of intracellular calcium. Through in vitro experiments, it has been found that temporal and spatial variation of shear stress is also important in addition to magnitude of shear stress.[32, 33] Bovine aortic endothelial cells within a confluent monolayer change their shape from polygonal to ellipsoidal and become uniformly oriented with the flow when exposed to laminar shear stress between 8 and 15 dynes/cm^2 for 24 hours.[34] Oriented cells begin to lose their elongation after the shear stress is removed and morphology of the monolayer is comparable to the unstressed controls by 72 hours.[31] It has been shown that laminar shear stresses decrease the adherence of both platelets and monocytes to the endothelial surface[35],

stimulate endothelial secretion of tissue plasminogen activator[36], increase endothelial mRNA levels[37], increase the release of endothelial intracellurlar calcium[38] and alter the genetic growth program of cultured endothelial cells inhibiting DNA synthesis.[39]

1.5 Objectives

The difficulties in detecting unruptured aneurysms in asymptomatic patients practically preclude the possibility of preventing most *subarachnoid hemorrhage*. It is highly desirable to be able to determine whether a particular aneurysm has a high risk of rupture so that it can be treated before bleeding occurs. Aneurysms of a larger size (>10 mm) and/or a higher aspect ratio (>1.6) have a high risk of bleeding.[40-42] However, the majority of the unruptured aneurysms do not meet these criteria,[41] and it is difficult to predict the likelihood of their rupture. An even more challenging task is to uncover hemodynamic and physiological environments that initiate aneurysmal growth. Recent research by our group has implicated high wall shear stress and positive wall shear stress gradient as aneurysmogenic-type hemodynamics. However, the effect of this hemodynamic combination on the endothelium has not yet been studied. Therefore, the objective of this work was to design a flow device to achieve specific combinations of wall shear stress and wall shear stress gradient values (positive and negative), followed by experiments to understand the response of endothelium to such hemodynamic environments.

CHAPTER 2

DESIGN OF *IN VITRO* FLOW SYSTEM

2.1 Objectives

The goal of the *in vitro* study was to replicate the physiological shear stress gradients in the endothelium to study the effects of positive and negative wall shear stress gradients. The flow system must also have regions of zero gradient to compare the effect with non zero gradient regions. This section describes, in detail, how the flow chamber was designed to meet this objective.

First, it was very important to determine the values of wall shear stress gradients that should be achieved, so that the flow system can mimic the real flow at bifurcations, as closely as possible. Next, an analytical treatment, based on loose assumptions, was used to design a flow chamber featuring converging and diverging height flow channel in which shear stress gradient (positive or negative) would be approximately constant along the line of the symmetry of the channel and large ranges of shear stress magnitude would be covered. Computational Fluid Dynamics (CFD) was used to calculate the actual shear stress distribution in the channels. The shear stress field was found identical to the analytical results, except at the regions very close to the side wall, which can be neglected. CFD was also performed for different flow rates to obtain a range of possible shear gradients. The final chamber has four different sections: (a) low WSS (b) high WSS (c) constant positive WSSG (d) constant negative WSSG. This allows us to study the effect of positive WSSG and negative WSSG, and also compare it with the results from

regions of zero gradient, in a single run of the experiment. Hence, number of experiments required is greatly reduced and effect of change in conditions with different experiments is avoided.

2.2 Study of Existing Flow Systems

Because of many questions regarding how endothelial cells mechanotranduce fluid shear stress into intracellular responses, the endothelial cell response to different flow conditions continues to be an active area of research. Although there have been significant advances in this field with animal models, *in vivo* work presents a number of challenges. In addition to difficulties associated with isolating the effects of mechanical signals caused by blood flow from the chemical humoral effectors, it is also difficult to visualize various force fields within the vasculature and to relate those stresses to specific endothelial cell phenotype in real time. Therefore, *in vitro* methods have been designed to mimic *in vivo* forces for the study of flow-mediated signaling in endothelium. Here, we will discuss the mostly commonly used methods to subject cells to different flow conditions.

2.2.1 Parallel plate flow system

The most common type of flow chamber system is the parallel plate type, where cells are introduced in a laminar flow field between two flat surfaces. Parallel plate flow chambers are used in dynamic studies of endothelium response to well-defined shear forces. Cultured cells are subjected to unidirectional shear stress in steady or pulsatile laminar flow. The channel height and flow rate, measured directly or calculated from pressure gradient between entrance and exit, determine the shear stress imposed upon the endothelial monolayer. This chamber is widely used

because it has many advantages: a) the device is simple in design, assembly, and operation and b) the endothelial cells can grow under flow conditions, and can be observed under microscope, or visualized in real time. One disadvantage is that it is difficult to discriminate between effects caused by shear stress and those caused by hydrostatic pressure, since both of them increase in a manner proportional to the flow. Furthermore, it is not possible to study effect of spatial gradients of shear stress on endothelial cells.

$$\tau = \frac{6\mu Q}{wh^2}, \quad \mu - \text{viscosity}; \quad w - \text{width}$$

Figure 5. Parallel Plate Flow Chamber

2.2.2 Cone and plate flow system

Cone and plate viscometers, also known as Couette flow devices, have been extensively used to impose a predetermined shear stress on cultured endothelial cells, and study its effect on cell phenotypic and functional traits. Figure 5. illustrates a typical layout of this apparatus. The system consists of a stationary flat plate, which is bottom of a cylindrical container, and a rotating, inverted cone. The cone is fabricated from non toxic material such as stainless steel, transparent polycarbonate, or transparent polymethylmethacrylate and attached to a gear that is driven by a variable speed motor. The cylindrical container is custom designed to either house a large diameter Petri dish, or snugly accommodate up to 12 circular coverslips lined with cells. To ensure laminar flow, the included angle between the cone surface and the flat plate is limited to

3^{o}. It is important to note that, in no case, laminar, turbulent or pulsatile, is the flow in the apparatus mimicking a physiologic situation in the vasculature. It merely provides a well defined biologic model for studying, *in vitro*, cellular response to flow induced forces. Moreover, wall shear stress is a function of angular velocity only and is constant at the test section, hence this device cannot be used to study spatial gradients of wall shear stress.

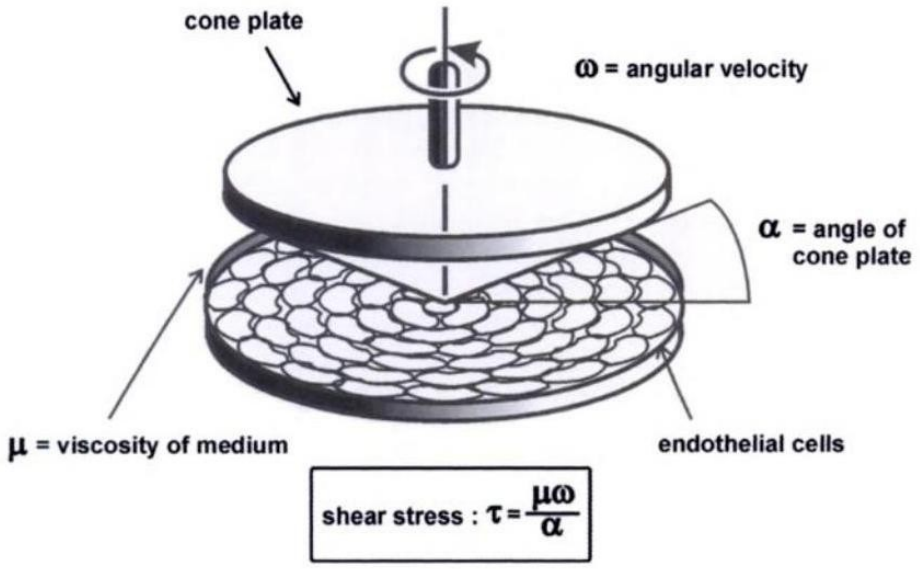

Figure 6. Cone and Plate viscometer

2.2.3 Step Chamber

If a small obstruction is placed in a parallel plate channel or cone and plate system, flow is disturbed immediately downstream the obstruction. Further downstream, uniform laminar shear stress is reestablished. High WSSG values can be achieved but for a very small distance. Moreover, it is difficult to control this distance and WSSG values.

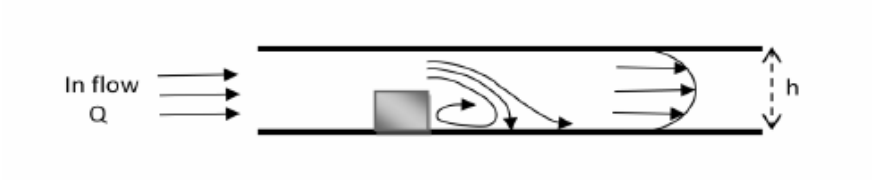

Figure 7. Step Chamber

2.2.4 Radial flow chamber

In a radial flow chamber, fluid is introduced in the centre, moves out radially and exits at the edge. So the radial flow apparatus provides an axisymmetric laminar flow field between two parallel disks. In this geometry, the cross-sectional area for flow between the two disks increases radially and the radial velocity decreases. Thus the wall shear stress decreases radially and this produces a continuous range of shear stress values within a given experiment. Again, constant wall shear stress gradients cannot be achieved in this device.

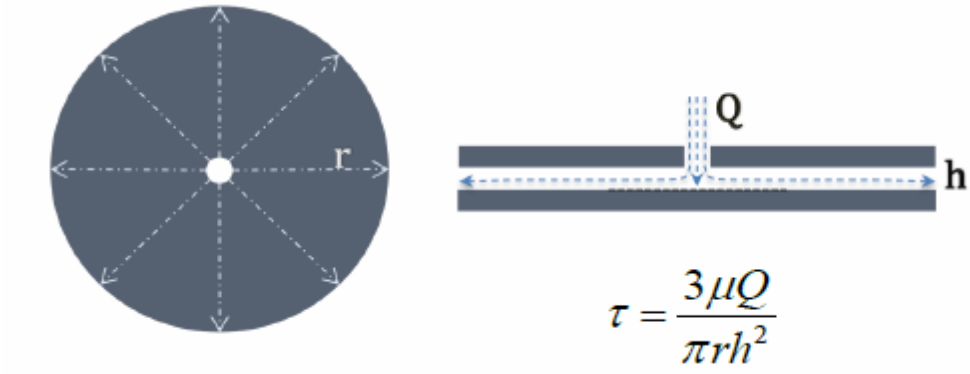

Figure 8. Radial Flow System

2.2.5 Stagnation point flow chamber

In all the flow chambers previously described, the adhesive surface is placed parallel to the flow direction. In a stagnation point flow chamber the endothelial cells are placed

perpendicular to the flow, providing a maximal medium/vessel wall contact. High wall shear stress and wall shear stress gradient values can be achieved but values are not constant for a substantial area which would be enough to make a meaningful study of effects of constant wall shear stress gradients.

2.2.6 Capillary perfusion chamber

A glass capillary tube is coated with collagen or another purified matrix protein and perfused with blood. The advantage of this approach is that, due to the very small diameter of tube, very high shear rates can be reached.

None of the flow systems described above provides hemodynamic forces which involve constant shear gradients, which is the focus of this research. Hence, there was a need to develop a new system to achieve constant shear stress gradients.

2.3 Determination of values of shear stress and gradients to be studied

Physiological values of wall shear stress gradients in human basilar artery bifurcation were found to be around 1200 dyn/cm^3. It is very difficult to achieve these values in an *in vitro* device for the following reasons.

i. By the definition of WSSG, a very high value of WSSG means a rapid increase in WSS with distance. Endothelial cells may not withstand very high values of WSS (>400 dyn/cm^2). A very high WSSG values can be applied only for a very small distance after which wall shear stress would harm the cells and hence limiting the maximum area of test section. But this area of test section cannot be less than the minimum required to make a

meaningful study. This area is limited by number of cells and cell density on the coverslip.

ii. Increasing the flow can increase the WSSG and WSS values. But flow becomes turbulent at higher flow rates. Hence a compromise has to be made for flow rate to keep the flow laminar throughout.

iii. Making the device thinner can increase the WSSG and WSS but manufacturability of CNC machining limits the minimum height achieved.

2.4 Theoretical flow chamber design

A parallel flow channel offers a constant shear stress region. A parallel channel can be modified (by changing height or width) to obtain variable shear stress distribution. A particular height or width variation can be found with the help of calculus, for which shear stress will grow or fall linearly, i.e. the shear stress gradient is constant in this region. The goal of flow chamber design was to achieve regions of constant wall shear stress gradients, this can be done using a converging (positive WSSG) and diverging (negative WSSG) channel.

To obtain the shear stress distribution for a converging channel we first consider the flow in a parallel channel. The analytical solution for the shear stress, τ , in a parallel channel is given by

$$\tau = \frac{6\mu Q}{wh^2} \qquad (1)$$

where w is the width of the channel, h is the height of the channel, μ is the viscosity of the fluid, and Q is the volumetric flow rate. This equation is valid for fully developed Newtonian flow and

$w >> h$. This equation is assumed to be valid for a converging channel. CFD results will show if this approximation is justified; if not, required changes can be made. $\frac{\partial \tau}{\partial x}$ is the spatial shear stress gradient along the flow where x is the dimension along the length of the channel. From the chain rule of differentiation we get

$$\frac{\partial \tau}{\partial x} = \frac{\partial \tau}{\partial h}\frac{\partial h}{\partial x} \qquad (2)$$

Using equation (1)

$$\frac{\partial \tau}{\partial h} = -\frac{12\mu Q}{wh^3} \qquad (3)$$

Substituting equation (3) in equation (2)

$$\frac{\partial \tau}{\partial x} = -\frac{12\mu Q}{wh^3}\frac{\partial h}{\partial x} \qquad (4)$$

Solving for $\frac{\partial h}{\partial x}$,

$$\frac{\partial h}{\partial x} = -\frac{wh^3}{12\mu Q}\frac{\partial \tau}{\partial x} \qquad (5)$$

$$\frac{\partial h}{h^3} = -\frac{w}{12\mu Q}\frac{\partial \tau}{\partial x}\partial x \qquad (6)$$

With limits $h = h_o \; at \; x = 0 \; and \; h = h \; at \; x = x$, integrating the equation (6), we get:

$$h = \frac{h_o}{\sqrt{1 + \frac{w h_o^2}{6 \mu Q} \frac{\partial \tau}{\partial x} x}} \qquad (7)$$

For a required value shear stress gradient $\frac{\partial \tau}{\partial x}$, equation (7) gives the corresponding variation of height with distance, for a given flow rate, viscosity and dimensions at the inlet.

The flow rate Q could be varied as required. Increasing the flow rate increases the shear stress gradient along with shear stress. Viscosity is that of culture medium i.e. μ is 3.45 cp. Decreasing the width of the chamber could help increase the gradients even more but minimum possible width of the chamber was determined by the width of the available microscope slide (2.2 cm). Also, with much lower width the assumption of the two dimensional flow will not be valid anymore. Decreasing the height could also help increase gradients but considering design for manufacturability for CNC machining, minimum height was restricted to 0.1 cm. At the inlet the maximum height, h_o, was decided to be 0.3 cm, in order to achieve base level shear stress just before convergence and inlet velocity 0.45 m/s . At this flow rate shear stress gradient is 100 dyn/cm^3. Figure 8 shows the corresponding design for shear stress gradient of 100 dyn/cm^3. Upper plot shows the height variation with length to achieve required shear stress distribution and the lower plot shows corresponding theoretical shear stress distribution. The shear stress increases from 35 dyn/cm^2 at the inlet to 285 dyn/cm^2 at the exit as the height decreases from 0.3 cm to 0.1 cm through a length of 2.5 cm. Regions before the inlet and after the exit are constant shear stress regions, each of length 5 cm. The same chamber can be run in the opposite direction (reverse flow) to achieve similar hemodynamics i.e. shear stress distribution but with negative

gradient. Thus, converging and diverging channels can be put in series to obtain multiple regions of positive and negative gradients.

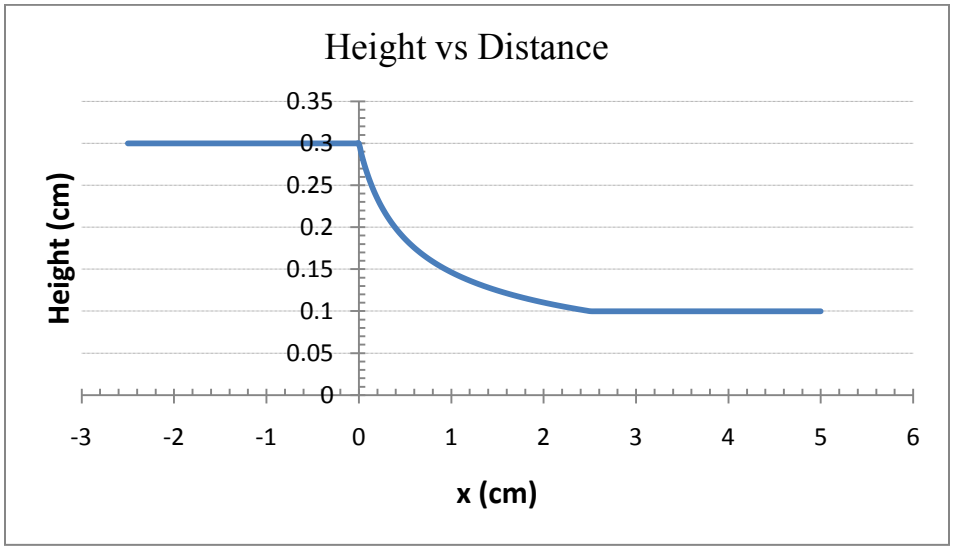

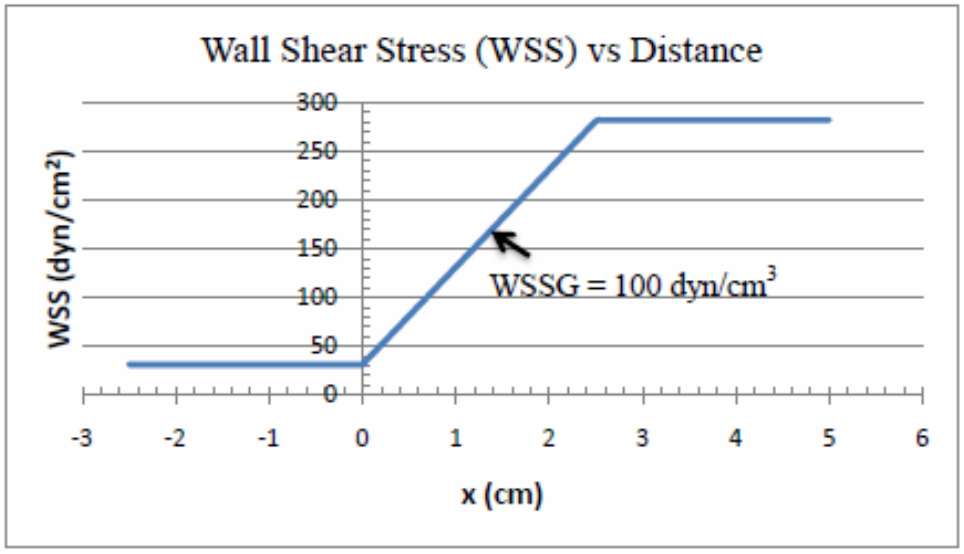

Figure 9. Theoretical design of chamber

2.5 Application of CFD to Optimize Conditions

For the initial design of the chamber, the assumptions of $w >> h$ and fully developed flow are not strictly satisfied. So, the real flow in the chamber is likely to differ from the analytical solution. To study this divergence or analyze the consequences of making these assumptions, Computational Fluid Dynamics simulations were performed on the initial design. These simulations were also important in refining the design to get to the required shear stress conditions.

CFD in the initial design (converging)

The 3D model of initial design was generated in Pro Engineer. The contour was defined by the equation (7) as input for the curve by equation option in Pro Engineer. The remaining edges were geometrically added to match the appropriate dimensions of the chamber. This 2D geometry is extruded normal to the plane, by the required width to achieve final 3D model. Parallel sections were limited to 2.5 cm on each side of converging section to save the number of nodes and computation time.

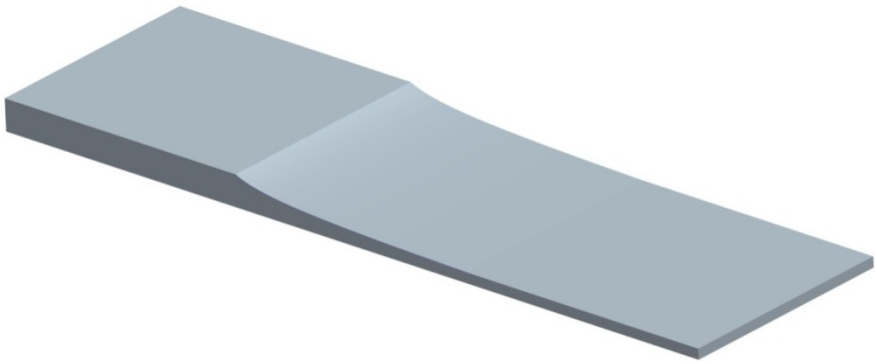

Figure 10. Intial 3D model designed in Pro Engineer

3D meshes were generated using ICEM-CFD (ANSYS Inc.). Different kinds of mesh elements were tried before concluding that extruded quad meshes gave the most effective mesh. The tetrahedral mesh did not give uniform elements near the boundary, which is important to study the wall shear stress accurately. The mesh size varied smoothly from larger elements near inlet (wider region) to smaller elements approaching the exit (thinner region). Also smaller elements were used to capture the converging contour accurately. CFD computations were done for different element sizes until a range of size was found where results were mesh independent i.e. moderate variation in mesh size did not affect the results. The final mesh resulted in 294,208 elements. The meshes are shown in Figure 9. and Figure 11.

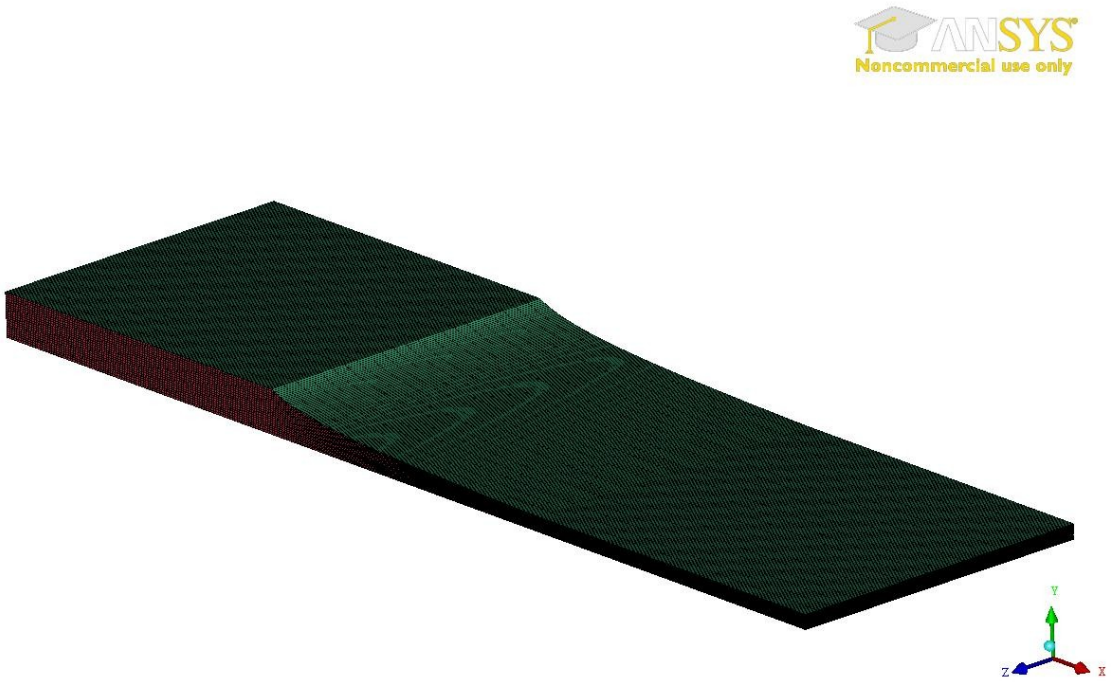

Figure 11. Meshed 3D model; mesh generated in ICEM-CFD

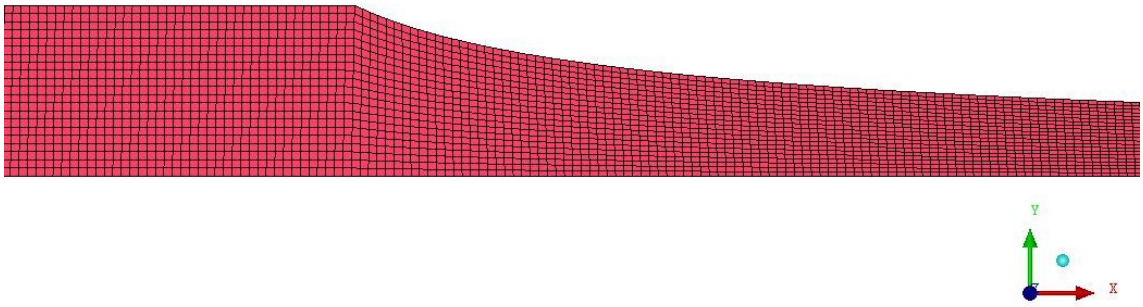

Figure 12. Side view of the mesh shows how mesh density increases in thinner sections.

The CFD simulations were performed using STAR-CD. Computations were run on a workstation equipped with 8 CPUs each with 3.2 GHz Intel Processor and 8 GB RAM. The fluid was modeled as a Newtonian fluid with viscosity 3.45 cp and a density of 1020 kg/m^3. The boundary conditions used were constant inlet velocity and zero velocity at all the walls. It is essential to specify no-slip boundary condition after specifying the inlet velocity to prevent a non-zero velocity into the wall surrounding the inlet. All the nodes on the wall facing the inflow must have zero velocity, making it consistent with the following nodes which will have zero velocity by the virtue of no-slip boundary condition. The inlet velocity was calculated by dividing the desired flow rate by the area of the inlet.

The computation was run with maximum number iterations 2000 and maximum residual error 10^{-9}. The flow results from STAR-CD were exported to TECPLOT. Shear stress magnitude

and shear stress gradient distribution along the centerline is plotted in Figure14. Calculated shear stress was found to be identical to analytical solution, except very near to the side wall. This was due to the assumption of 2D flow or $w >> h$. This divergence from analytical solution was prominent only in a very small region close to the wall. At the start of the convergence, gradient slowly increases following which it remains fairly constant. Shear stress grows from 35 dyn/cm^2 to 285 dyn/cm^2 through a nearly constant positive gradient of 106 dyn/cm^2.

CFD computation was also done for the reverse flow. Though similar hemodynamics was expected with reverse flow but it was important to check possible recirculation zones. Shear stress distribution is plotted in Figure 15. Shear stress falls from 285 dyn/cm^2 to 35 dyn/cm^2 through a nearly constant negative gradient of 97 dyn/cm^3. No major recirculation zones were found under the desired flow conditions. A small one seen near the top end (divergence end) did not affect the wall shear stress on the bottom surface.

2.6 CFD Results

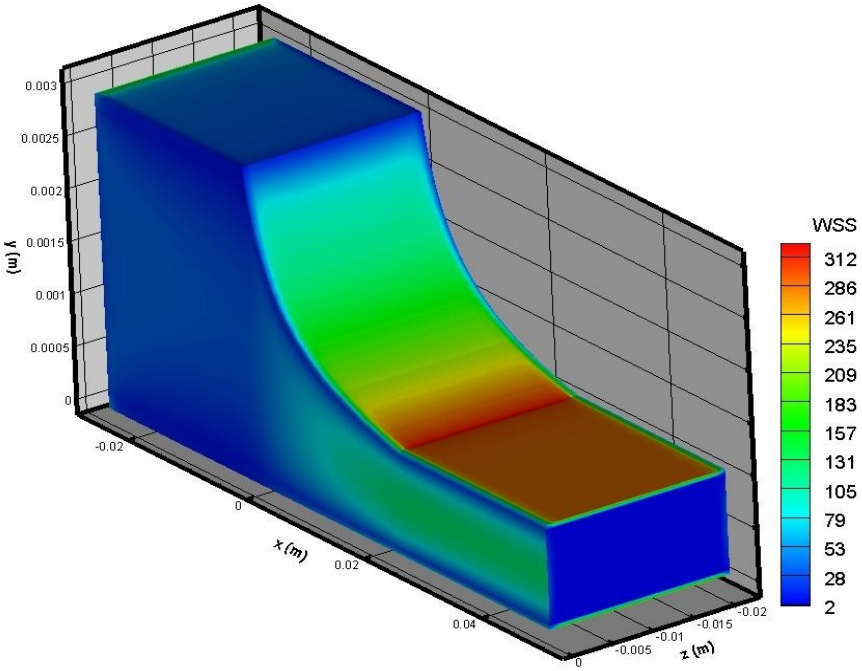

Figure 13. WSS contours on the chamber surface

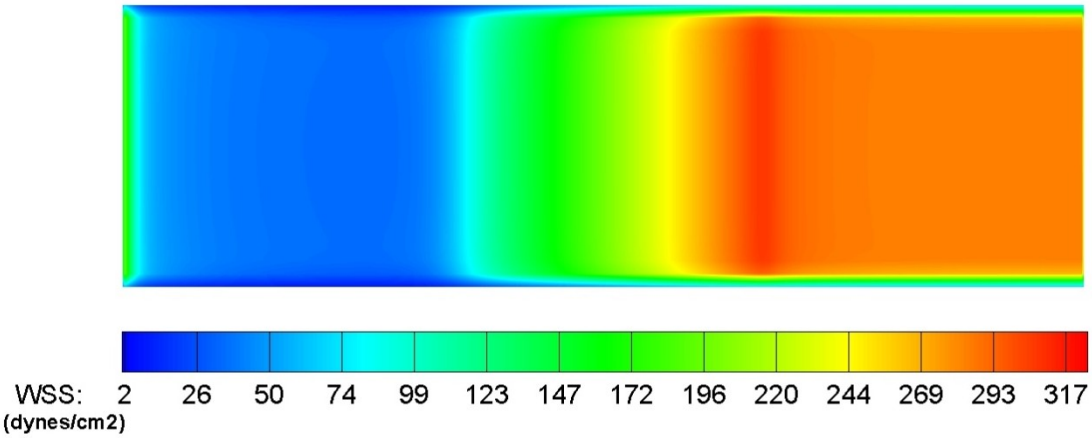

Figure 14. WSS contour along the chamber base

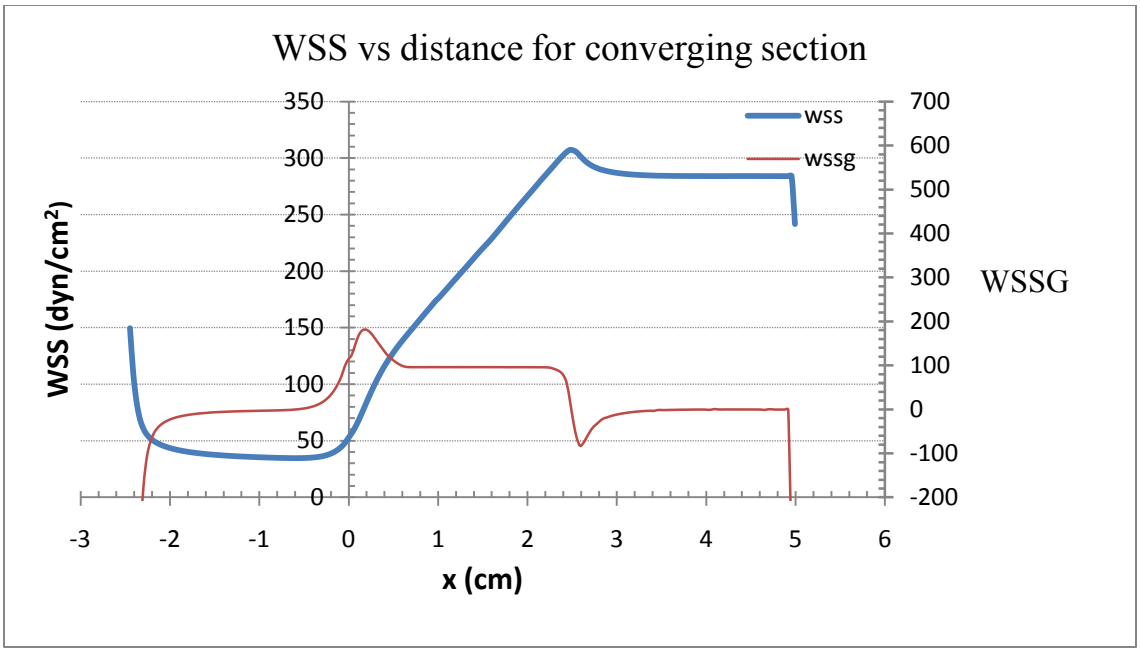

Figure 15. WSS and WSSG variation on the chamber base (converging section)

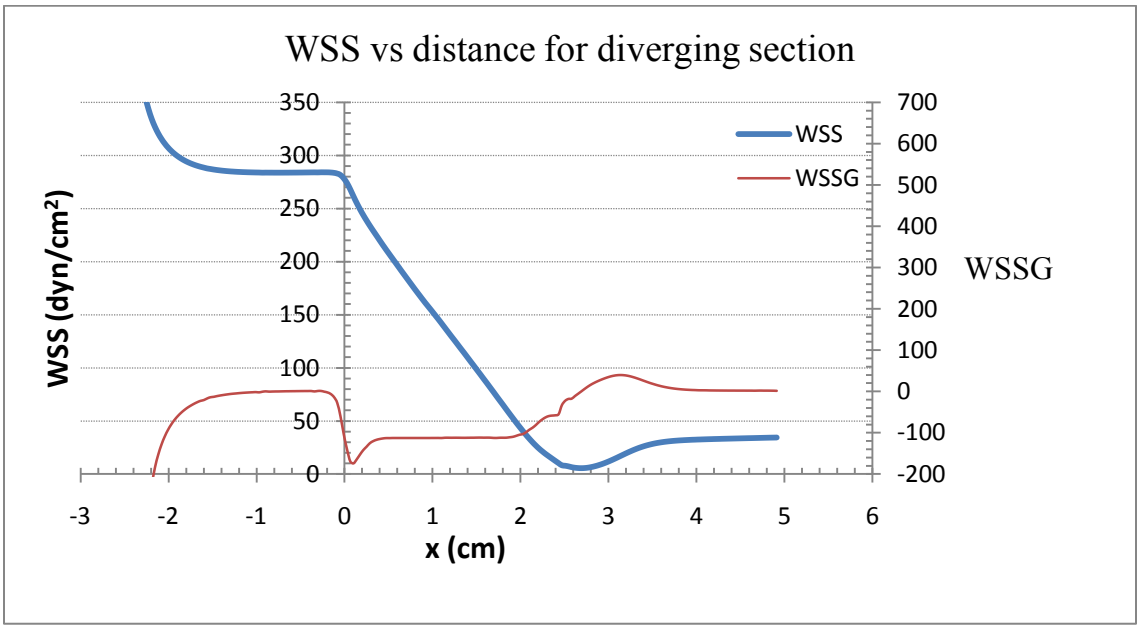

Figure 16. WSS and WSSG variation on the chamber base (diverging section)

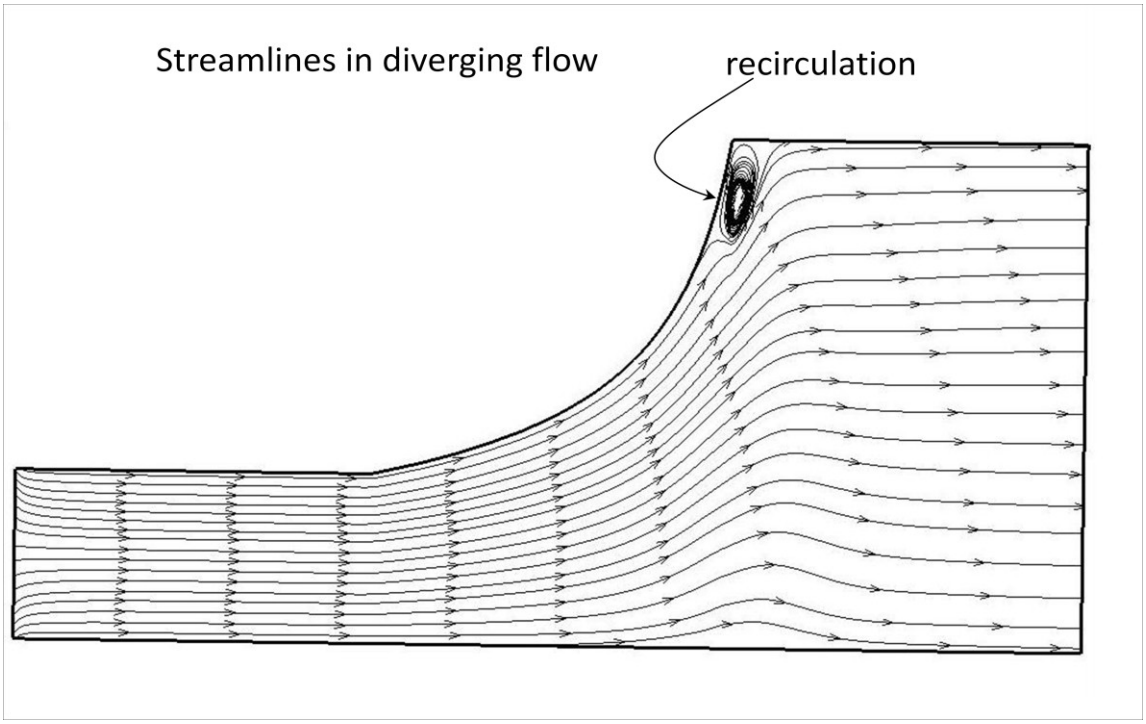

Figure 17. Streamlines in the diverging section

Figure 12 shows the WSS distribution on the surface of the chamber. The result shows that WSS is uniform throughout the width, hence the 2D approximation is justified. Figure 13 shows the WSS distribution on the bottom surface, which is primarily the test section. The flow develops very rapidly as just following the inlet the WSS magnitude becomes uniform at base level. Again Figure 13 shows that edge effects due to side wall are prominent only to a very short distance and hence can be neglected. Similar CFD results were also obtained for diverging section defining the flow in opposite direction for the same model. Magnitude of WSS and WSSG at centerline are plotted against the flow direction for converging and diverging section in Figure 14 and 15, respectively. Figure 16. shows the streamlines, a small recirculation zone can be observed near the top end , at the end of divergence.

2.7 Joining the chambers in series

Two converging and two diverging chambers were joined in series to get multiple regions of positive and negative shear stress gradients. The connections were kept long enough so that the flow is fully developed before entering a new section i.e. it prevented any possible changes in flow dynamics due to connections. Figure 17. shows one converging and diverging chamber in series and corresponding centerline shear stress variation. Connectors were added to the ends to allow a smooth entry for the flow. Small expansions were used to merge the flow from connecter to the inlet of the chamber. As the Reynolds number is small, flow develops rapidly and non uniformities in the expansions will not affect the shear stress distribution much. Hence, for CFD it was assumed that fluid enters the chamber with a uniform velocity.

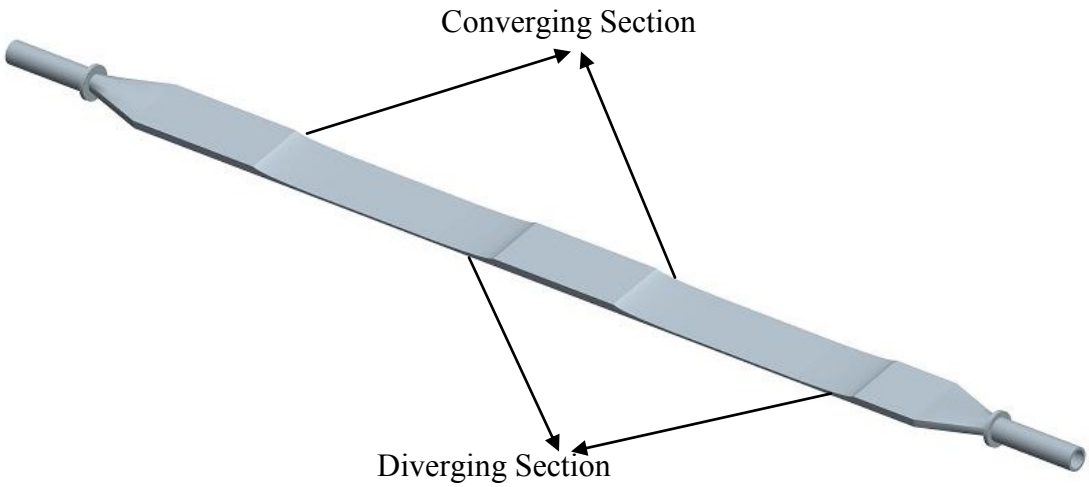

Figure 18. Final model of chamber with two converging and two diverging sections. Designed in Pro Engineer.

2.8 Flow chamber manufacturing

The geometry of the chamber was divided into two parts, upper and lower. Mold was manufactured for each part by machining the geometry from polycarbonate blocks. Silicone elastomer (Sylgard) was poured into the mold and left for 3 days to cure. For the bottom half, coverslips (50x22mm) were placed on the desired sampling location before pouring the silicone elastomer, to create a groove for cover slides to be placed while running the experiment. Autoclavable material was used for the chamber so that it could be assembled with the remaining components of the flow loop and then autoclaved as a closed system.

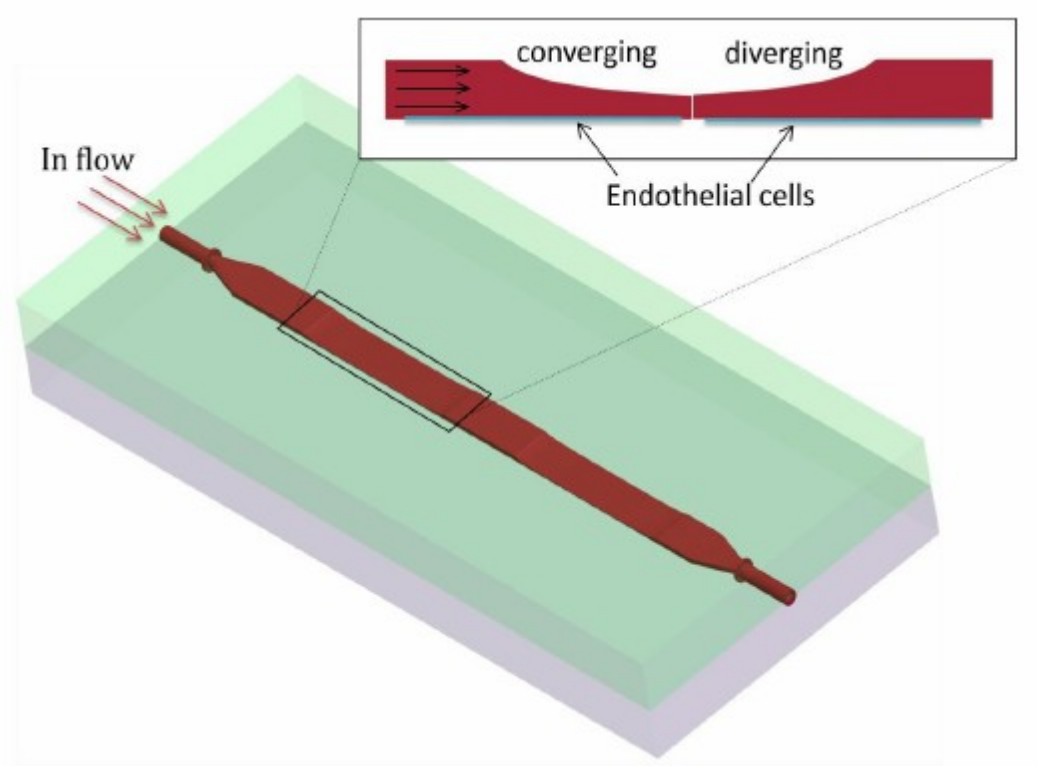

Figure 19. Placement of endothelial cells in the flow chamber and flow exposure. (Pro Engineer)

The two halves were put together to get the final chamber. Two thick polycarbonate plates with drilled holes were used to hold the two halves together. The grip could be secured by using screws with nut bolts through the holes to prevent any leakage. Connectors were manufactured from Teflon. When assembled the flow channel consists only of two openings through the connectors, inlet and outlet. For additional views and detailed engineering drawings of flow chamber, see Appendix A.

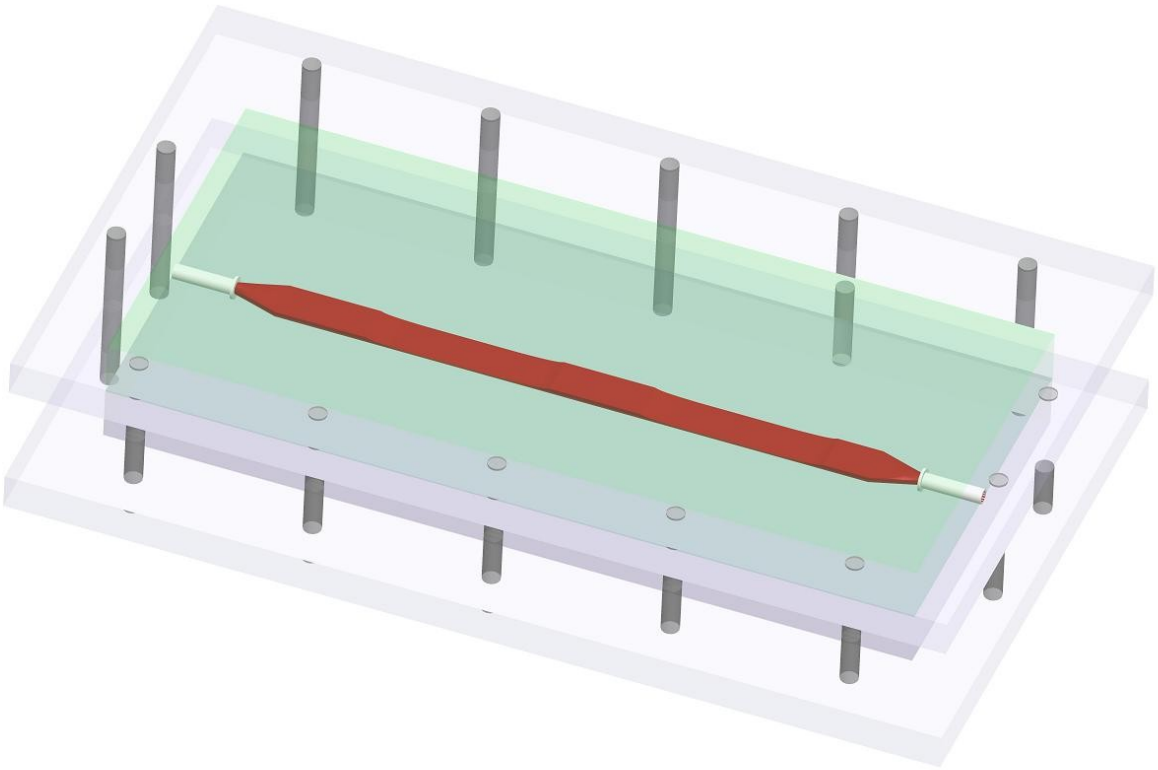

Figure 20. Flow chamber secured with polycarbonate plates and screws. (Pro Engineer)

2.9 Flow Loop Design

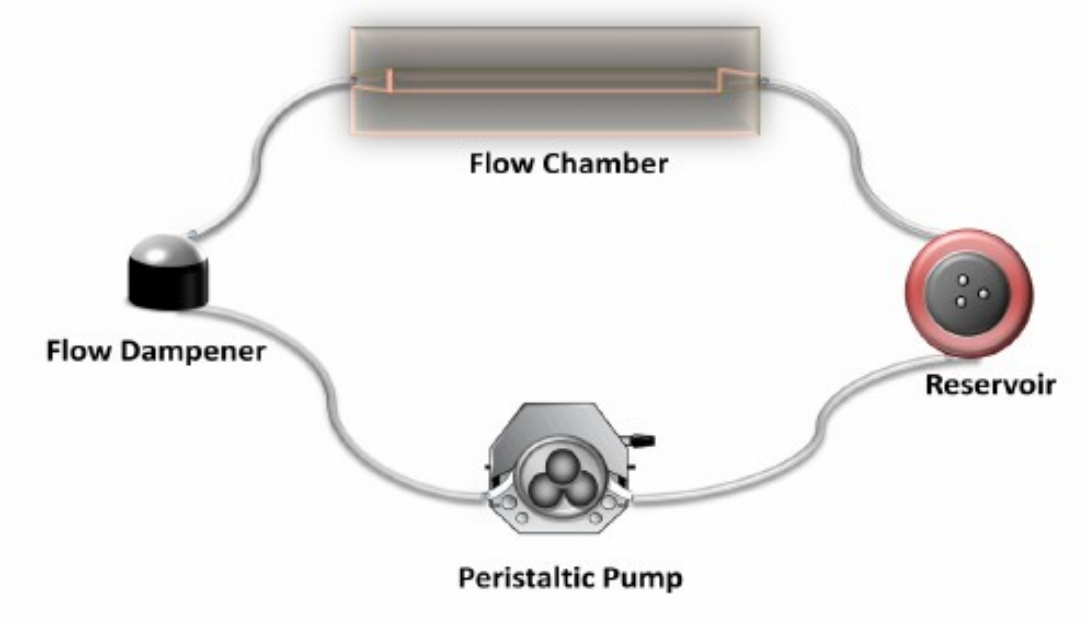

Figure 21. Flow Loop Design

An *in-vitro* flow loop is important to maintain a constant and known flow rate to the flow chamber, as required for each experiment. Bovine aortic endothelial cells (BAECs) were exposed to predefined WSS levels by placement in a flow loop consisting of a reservoir, a peristaltic pump, three dampeners, and the gradient chamber. The peristaltic pump was used to drive the flow, which draws flow media from a reservoir, which was open to atmosphere via a filter. To minimize spallation, Gore® Sta-Pure® tubing was used in the pump section. The fluid then passed through flow dampeners to dampen the pulsatility of the pump and then through the flow chamber. A pressure transducer (Becton Dickinson) was located just before the flow chamber to enable systematic pressure (static) measurement near the device, the pressure was set at 95$\pm$5 mmHg in all experiments. The flow rate is measured using a transit-time ultrasound flow probe

(Transonic Inc.), calibrated for silicone tubing and the perfusion media to measure the flow rate within. This probe could be placed at multiple locations along the flow loop to measure inlet and outlet flow rates at any point during the experiment. The primary tubing used was a nontoxic thermoplastic elastomer specially designed for cell culture work. All the components of the flow loop were sterilized by autoclaving. The entire system was housed in a single incubator, which was humidified, maintained at 37 $^{\circ}$ C, and equilibrated with 5% CO_2 to maintain a proper pH with the buffered culture medium.

The flow loop was assembled in a sterile biosafety cabinet. The coverslip containing BAECs was removed from its culture dish and sterilely placed in the flow chamber. The chamber was quickly assembled. The flow rate was gradually increased to the desired level while simultaneously tightening the screws just enough to prevent any leakage. Once the desired flow conditions were achieved, the flow system was transferred from biosafety cabinet to the incubator.

Details of flow loop components can be found in Appendix B.

CHAPTER 3

DESCRIPTION OF BIOLOGICAL ASSAYS FOR THE *IN VITRO* STUDIES

3.1 Cell Culture

Bovine Aortic Endothelial Cells (BAECs) between passages 15 and 16 were cultured on sterile 24 x 50 mm glass cover slips with Dulbecco's Modified Eagle's Medium (DMEM; Invitrogen) supplemented with 10% Fetal Bovine Serum (FBS; Invitrogen) and 100 U/ml penicillin and 100 μg/ml streptomycin (Invitrogen). The cell cultures were maintained in a humidified incubator at 37°C and 5% CO_2 and fed every 2 days until they reached confluence. Once confluent, they were equilibrated in flow media for 24 hours to allow the cells to adapt to the new media. Flow media consisted of DMEM, 5% FBS, 100kU penicillin, 100mg streptomycin, and 80 g Dextran 70 (GE Healthcare) per liter of media, which was used to match the viscosity of blood. Time-matched static controls were maintained under the same conditions but were not exposed to flow. Each experiment was performed in triplicate to obtain redundancy.

3.2 Experimental Protocol

All components of the flow loop were wrapped and sterilized by steam autoclave, before running the experiment. Once cooled, the loop was placed in a clean biosafety cabinet. The entire flow loop was assembled in the hood and flow media was added to the reservoir. The cover slips were then placed in the grooves of flow chamber. One end of each cover slip was marked to keep

track of its alignment in the flow. The top section of the chamber was placed and secured using stainless steel bolts.

The flow pump was immediately started to prevent the cell monolayer from drying out. Flow rate was gradually increased which was measured using the flow probe. Once the required flow rate was established, the pressure gauge and clamp were used to increase the pressure to a physiological level (95±5 mmHg). The entire flow loop was placed in an incubator at 37°C and 5% CO_2, to ensure stable temperature and pH for the duration of the experiment. Flow rates were monitored periodically. Experiments were run for 24 hours. A monolayer of cells cultured under the same conditions was placed in the incubator in a Petri dish with flow media (no flow) for the duration of the experiment and was used as a control.

After each experiment, the flow chamber was disassembled and the cell cover slips were removed and (with controls) immediately placed in fixative.

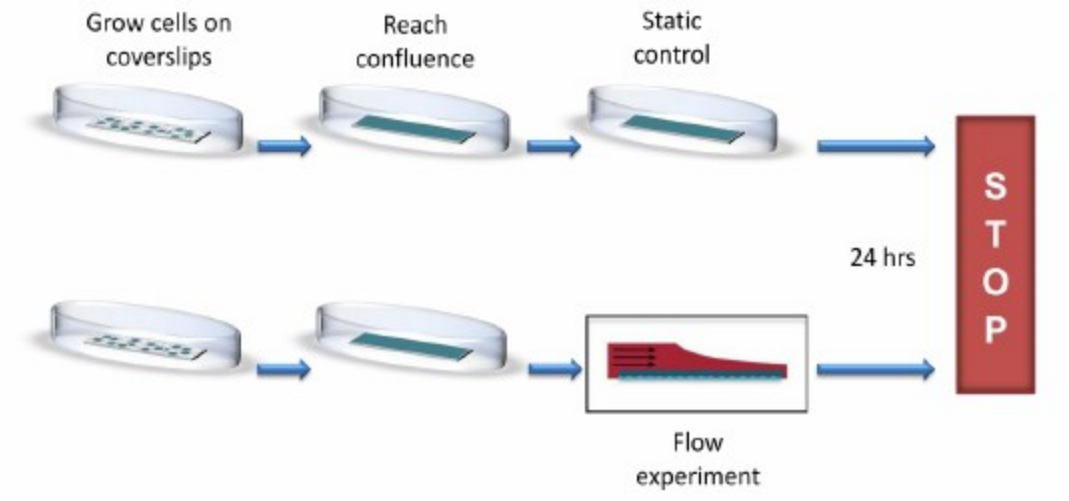

Figure 22. Experimental protocol

3.3 Morphological Examination

In order to spatially map the morphology of the cells in regions of different WSS, a composite image of the entire length of the EC monolayer was created by stitching together sequential images of the cells taken at 10x magnification. The edges of the coverslip (5 mm from each end) were excluded to eliminate areas of cell disruption due to handling. Images were acquired and assembled using a Zeiss Axioimager motorized fluorescence microscope and accompanying Axiovision software (Zeiss). Microscopic examination and description of the morphology (shape, size, and orientation) of the EC monolayer was achieved by observing the cells with an inverted phase contrast microscope (Zeiss Axiovert 40). Digital images were taken using an inverted microscope (Zeiss Axiovert 135) with a mounted CCD camera (Hamamatsu Orca-ER) and IPLab software.

CHAPTER 4

EXPERIMENTAL RESULTS OF IN VITRO STUDIES

Using the flow chamber, ECs were subjected to flow for 24 h. Light microscopic examination revealed a confluent monolayer of ECs for all values of WSS and gradient.

4.1 Cell Morphology and Alignment

To determine the cell orientation, the cell boundaries were traced manually and roughly 100 cells per image were analyzed quantitatively using ImageJ, an image processing and analysis software developed by the National Institutes of Health (NIH). Basically, each of the individual cells was represented by an ellipse that best fits the boundary of the cells. The direction of the major axis of the ellipse represents the direction or alignment of the cells relative to the flow direction and length of major axis represents size (elongation) of the cells. The alignment, elongation and different shape descriptors (circularity, aspect ratio and roundness factor) were calculated using tools in the ImageJ software. The image was calibrated using the known width of image from inverted phase contrast microscope (Zeiss Axiovert 40) for total pixels in image width.

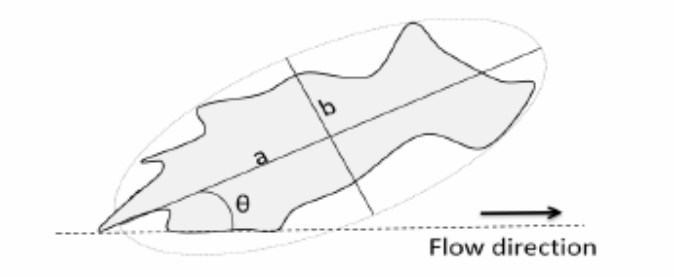

Figure 23. Illustration of measurement of alignment, θ and elongation, a.

Low WSS ≈ 35 dyn/cm^2

A.

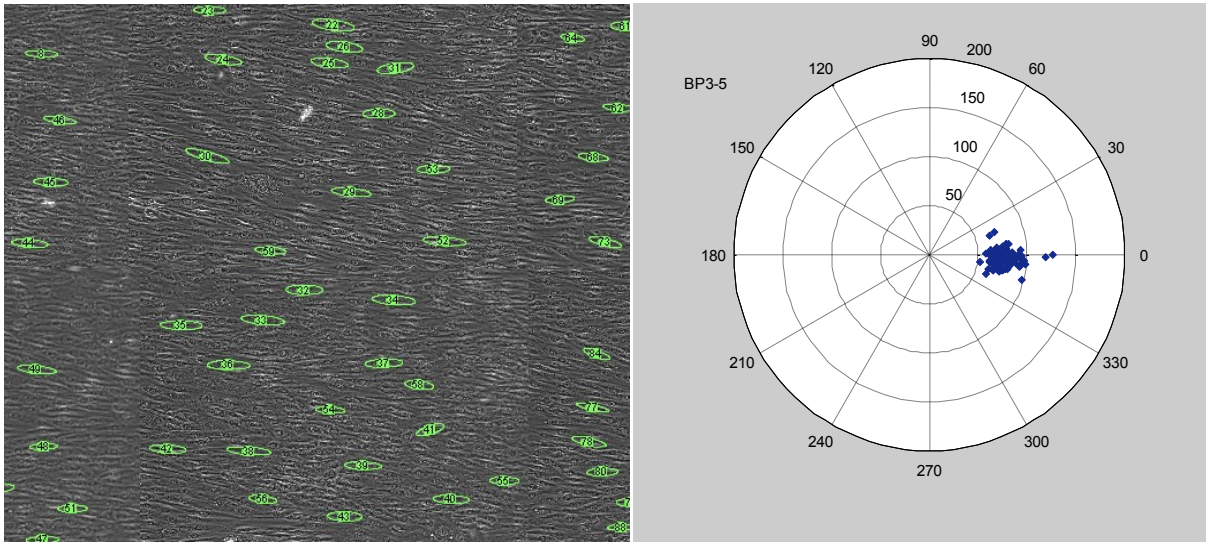

WSS ≈ 35 dyn/cm^2

B.

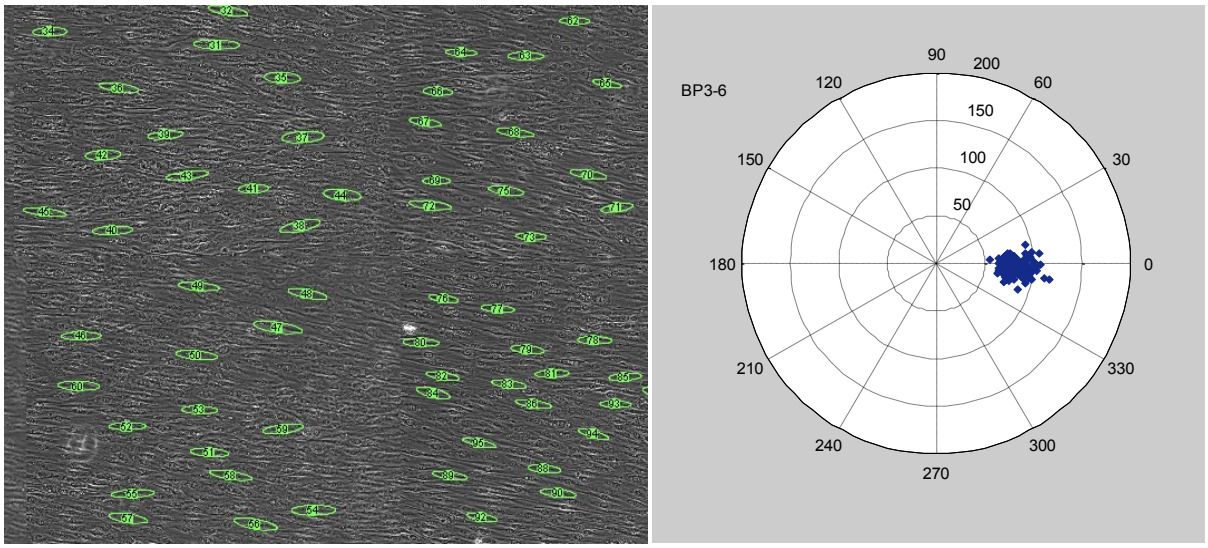

WSS ≈ 35 dyn/cm^2

Positive WSSG

C.

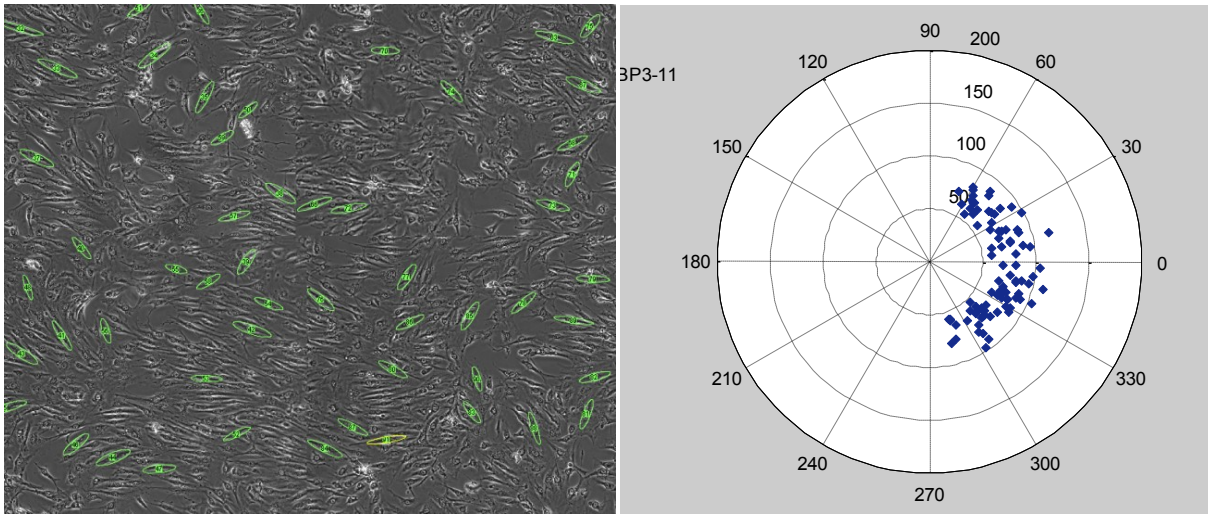

WSS ≈ 140-163 dyn/cm^2

D.

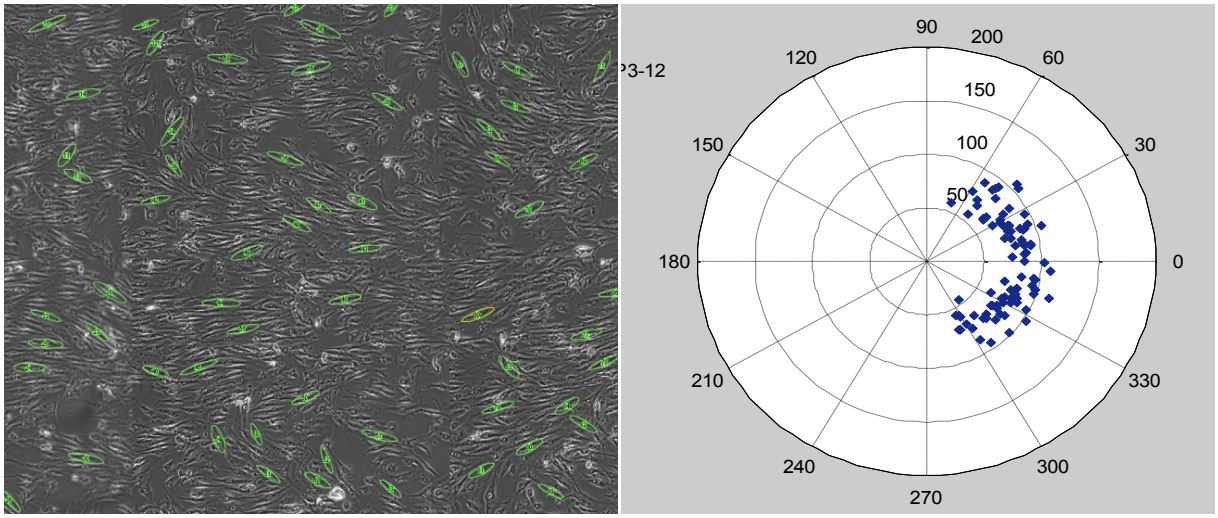

WSS ≈ 163-186 dyn/cm^2

E.

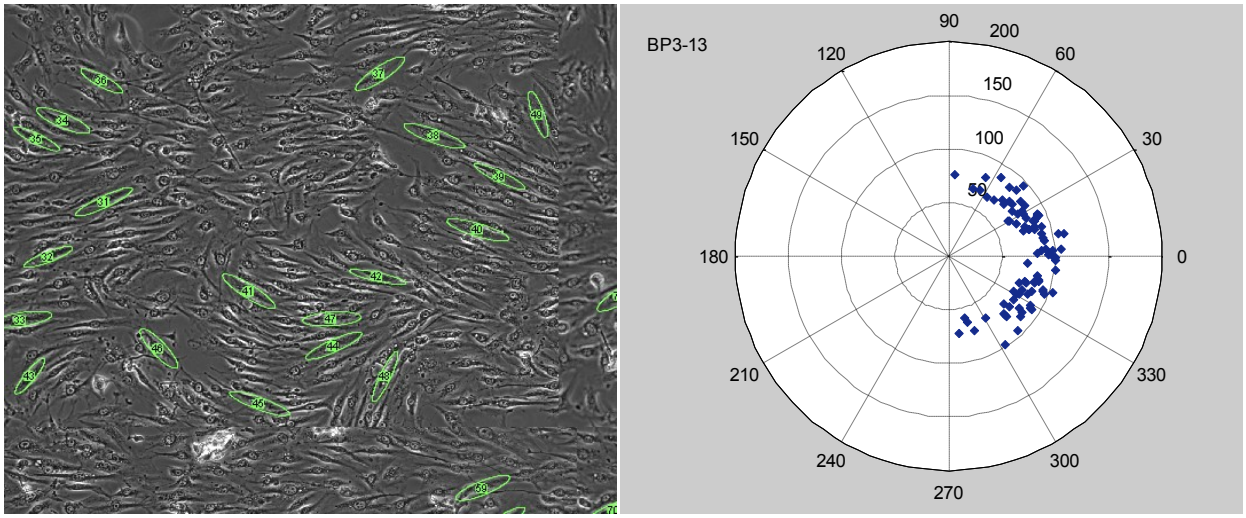

WSS ≈186-209 dyn/cm^2

Positive WSSG

F.

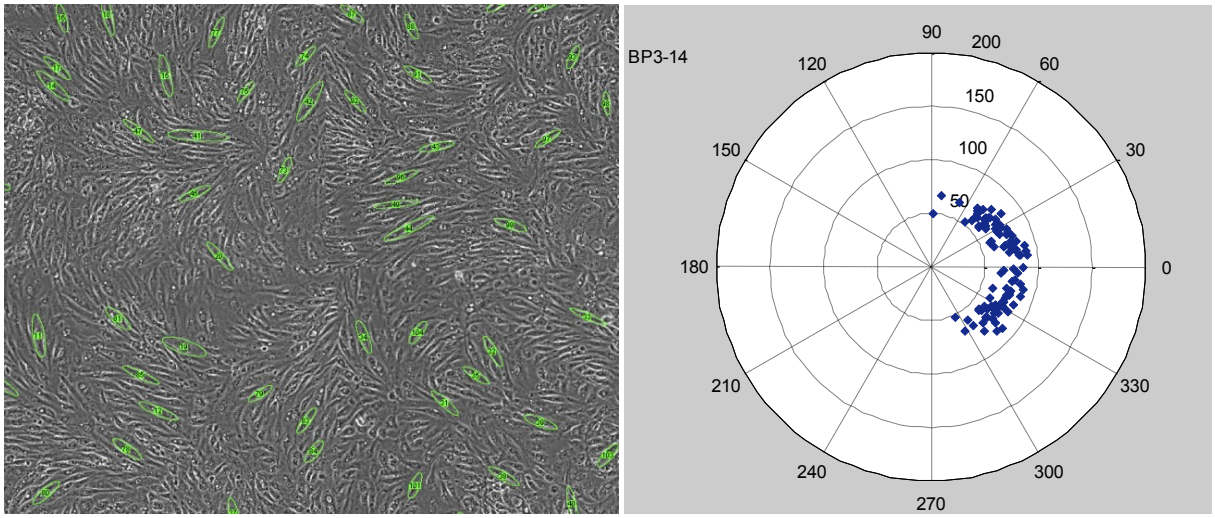

WSS ≈ 209-233 dyn/cm^2

Figure 24. Cell morphology (left) showing fitted ellipses and polar plots (right). Angles in polar plots are in degrees and radius in microns. A) & B) WSS ≈ 35 dyn/cm^2 ; C) WSS ≈ 140-176 dyn/cm^2; D) WSS ≈ 176-196 dyn/cm^2; E) WSS ≈196-220 dyn/cm^2; F) WSS ≈ 220-244 dyn/cm^2.

High WSS ≈ 285 dyn/cm^2

A.

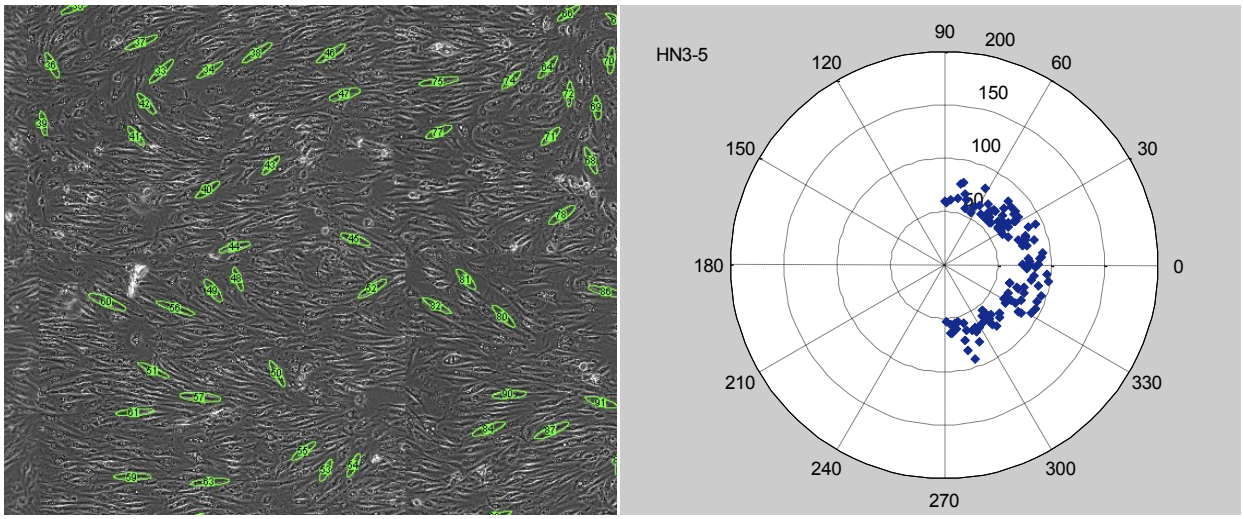

WSS ≈ 285 dyn/cm^2

B.

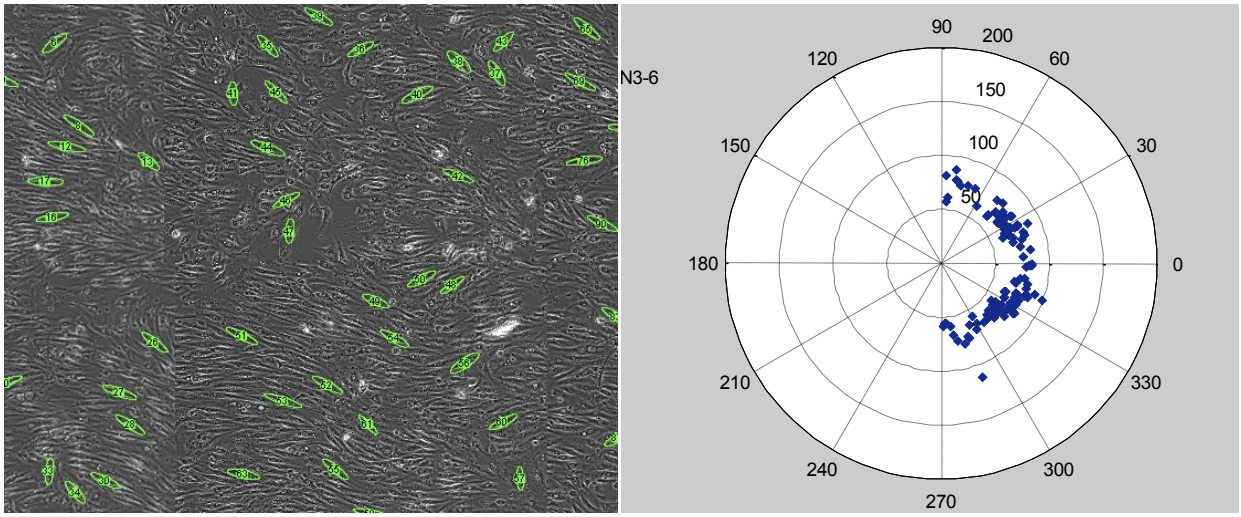

WSS ≈ 285 dyn/cm^2

Negative WSSG

C.

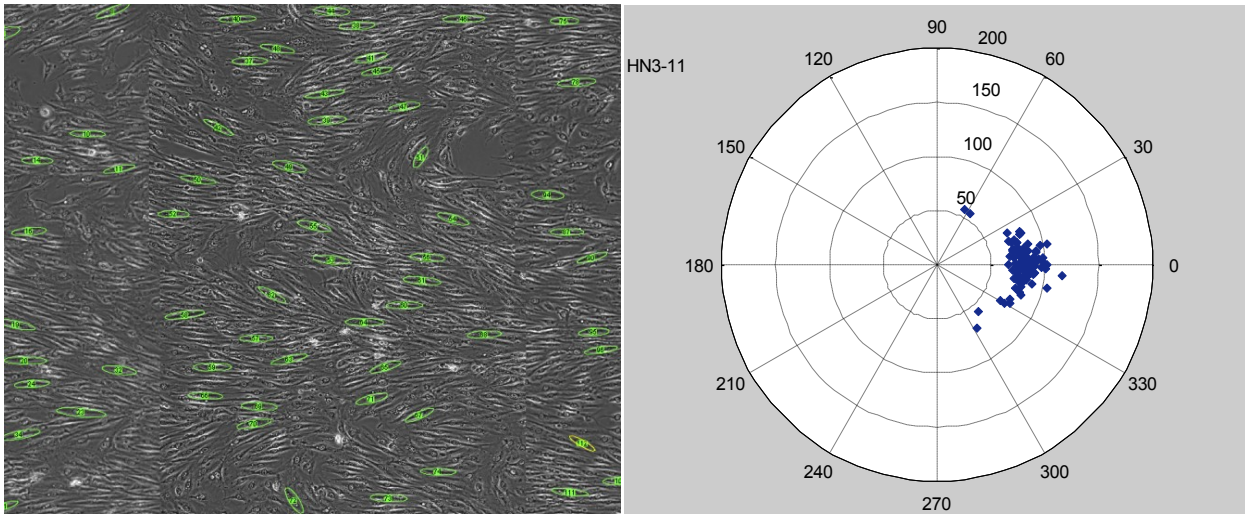

WSS ≈ 210-180 dyn/cm^2

D.

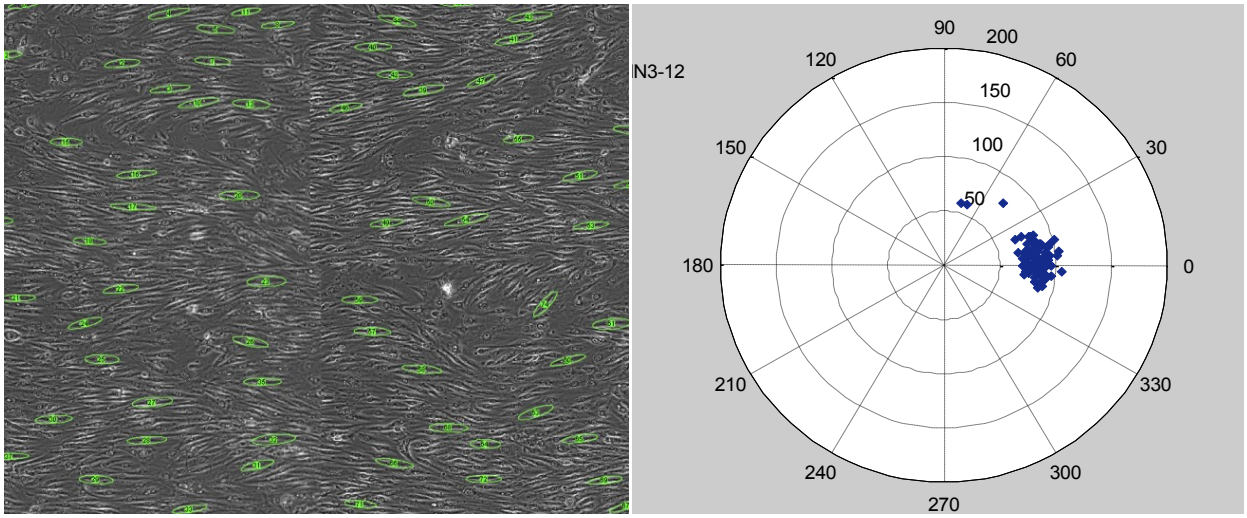

WSS ≈ 180-150 dyn/cm^2

E.

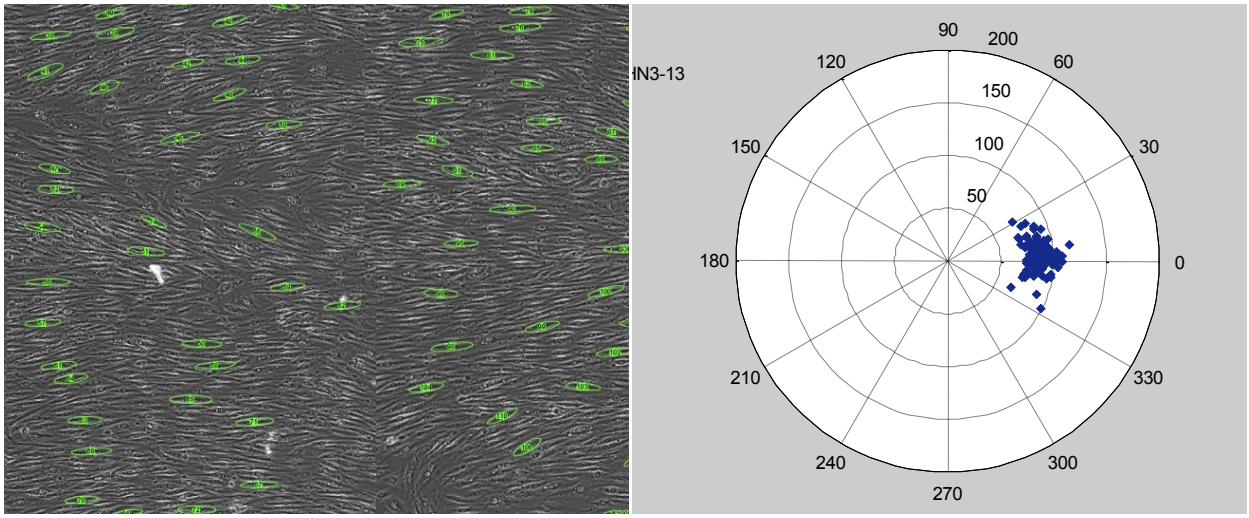

WSS ≈ 150-120 dyn/cm^2

Negative WSSG

F.

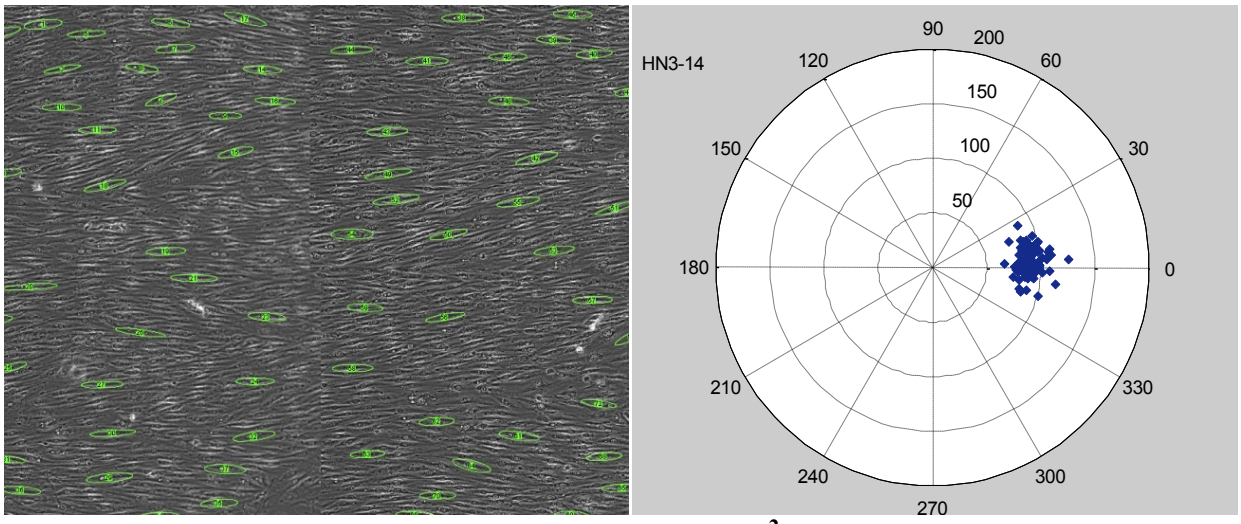

WSS ≈ 120-90 dyn/cm^2

Figure 25. Cell morphology (left) showing fitted ellipses and polar plots (right). Angles in polar plots are in degrees and radius in microns. A) & B) WSS ≈ 285 dyn/cm^2 ; C) WSS ≈ 210-180 dyn/cm^2; D) WSS ≈ 180-150 dyn/cm^2; E) WSS ≈150-120 dyn/cm^2; F) WSS ≈ 120-90 dyn/cm^2.

Comparison of results in positive and negative WSSG at same WSS range (150-210 dyn/cm^2)

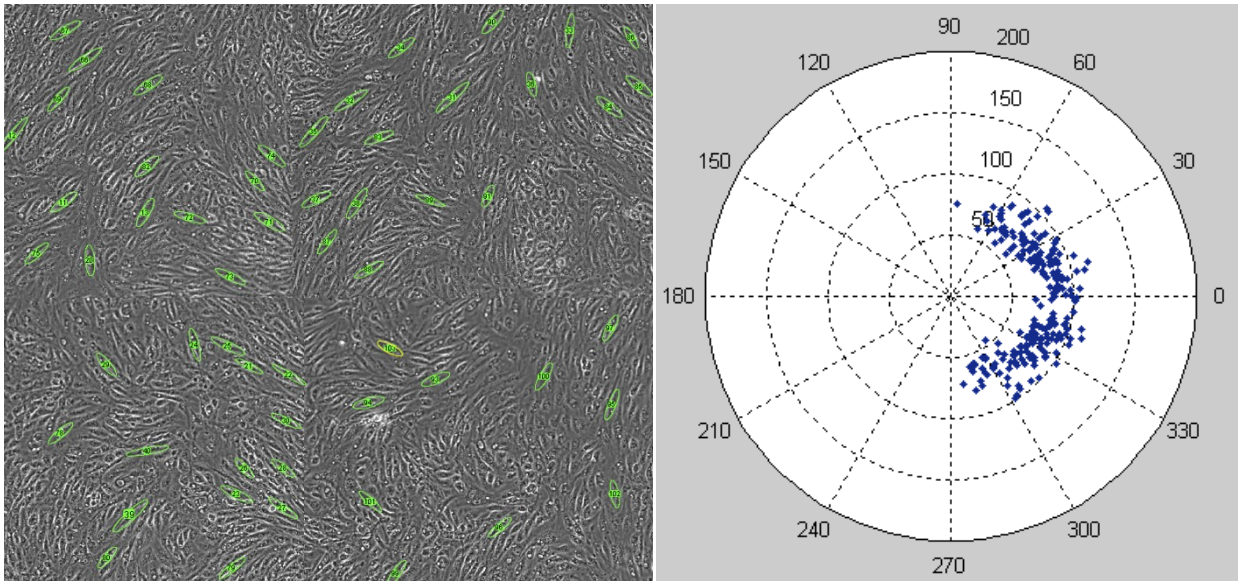

Positive WSSG

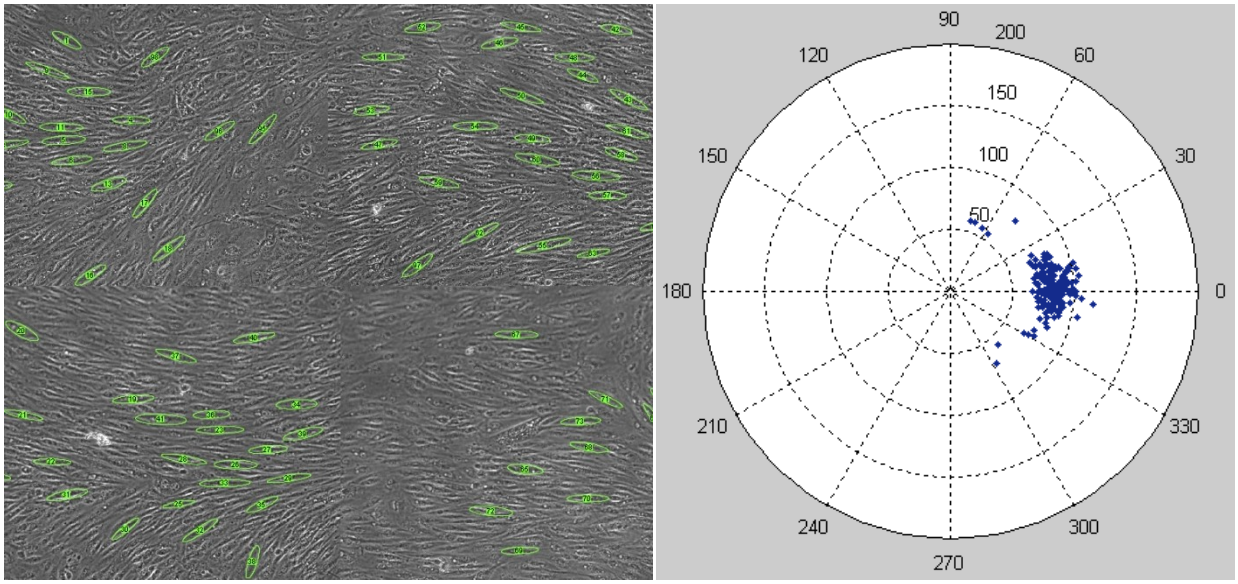

Negative WSSG

Figure 26. Comparison of positive and negative WSSG regions in same WSS range

In all flow environments cell alignment was nearly symmetric about the flow direction, which implies that the flow is uniform along the width as cells did not align in a preferred direction. It is also in agreement with our 2D flow assumption. As expected, at baseline wall shear stress ECs were elongated and aligned with the flow. In regions of positive WSSG the cells aligned at an average angle of 33^{o} from the flow direction. The alignment was found to be similar in all regions of positive WSSG irrespective of WSS magnitude.

In the regions with high WSS, ECs also aligned away from the flow as in the positive WSSG regions but at greater average angles of 40^{o} from the flow direction. Under negative WSSG conditions the EC alignment closely mimicked the alignment of the cells at the baseline WSS conditions, i.e. they primarily aligned parallel to the flow at small average angles of 8^{o}. The alignment in negative WSSG region was identical irrespective of WSS.

Cell elongation was also measured for all the cells studied for alignment. No significant difference was observed in elongation at all WSS and WSSG regions, the major axis of best fit ellipse for all cells was 50-100 microns. Other shape descriptors such as circularity, roundness and aspect ratio were also calculated for all selected cells, but those parameters remained identical at all different environments.

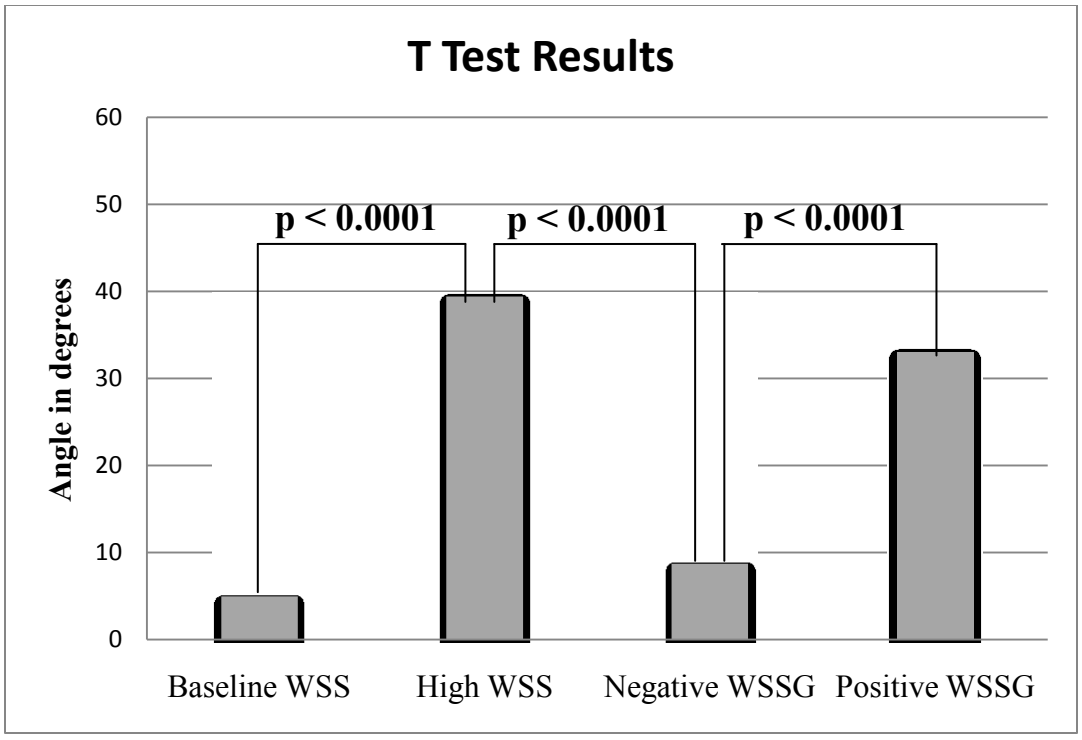

Figure 27. Student T test Results

Student T tests were also performed for all the regions to quantify the difference between degrees to which the ECs aligned with the flow. Very low p values were found which substantiate the observed high difference in alignment at all studied hemodynamic environments.

CHAPTER 5

CONCLUSIONS AND FUTURE STUDIES

While other studies have analyzed the effects of complex flow fields containing spatial shear stress and shear stress gradients on endothelium, this work is the first to isolate and compare the effects of positive and negative WSSGs on endothelial cells. This study focused on cell morphology changes under flow environments with different combinations of WSS and WSSG, and discuss what possible hemodynamics is responsible for damaged endothelium at the aneurysm sites. Based on the results, positive WSSG causes the ECs to align away from the flow direction or in other words the cells are not aligned with the flow. But under negative WSSG the cells align with the flow direction. The EC alignment is identical to the alignment observed in low WSS or baseline WSS regions. At higher WSS but zero gradient the cells are again non aligned. At high WSS the cells align nearly perpendicular to the flow. Results show that at ECs respond to negative WSSG as they do to baseline WSS with no gradient, hence low damage is expected in negative gradient regions. This is in agreement with our previous dog studies where no damage was found at negative WSSG as compared to positive WSSG at similar WSS.

The exact mechanism by which the ECs respond to WSS or WSSG is not known. Based on the findings in this study, the cells are able to respond uniquely to positive and negative shear stress gradients, this implies that the cells possess some global mode of sensing this hemodynamic phenomenon. One possible mechanism may involve intercellular communications, since neighboring cells in the presence of a spatial shear stress gradient will experience different forces.

Future Recommendations

Suggested Chamber Modifications

Through the course of running experiments and analyzing data for this study, a few areas of potential improvement, with regard to the efficiency of the chamber, have been noted.

The failure of shear stress gradient to rise to a constant value instantly was a deviation from the theoretical distribution of wall shear stress gradient. The gradient did not rise smoothly to the constant value, instead a sharp bump in WSSG was observed before it achieved the constant value. Though there cannot be a sharp jump in WSSG but iterative studies can be done to optimize the design for smooth transition to constant WSSG from zero WSSG. Design can also be modified to prevent any leakage by using O-ring.

In Vitro Experiment Suggestions

There is a high possibility that cell response will be different under the same flow environment but longer duration. The same experiments can be run for 48 hours to examine this possibility.

It is also likely that cells under a specific environment affect the cells downstream by release of substances or chemicals. The experiments can be run in a different configuration where a zero gradient region follows gradient region and then compare the response with a response from simple parallel plate flow channel experiment.

Proliferation, apoptosis, density and migrations can also be studied to get a better insight into the response of endothelium cells to different flow environments.

Appendix A : Flow Chamber Development

1. Design

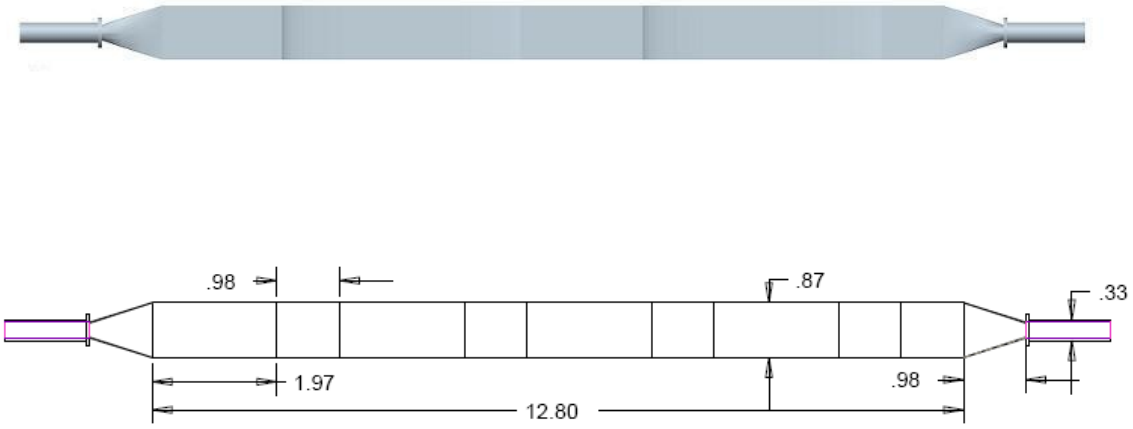

Figure 28. Top view of the chamber, which was designed using Pro Engineer. Dimensions are expressed in inches.

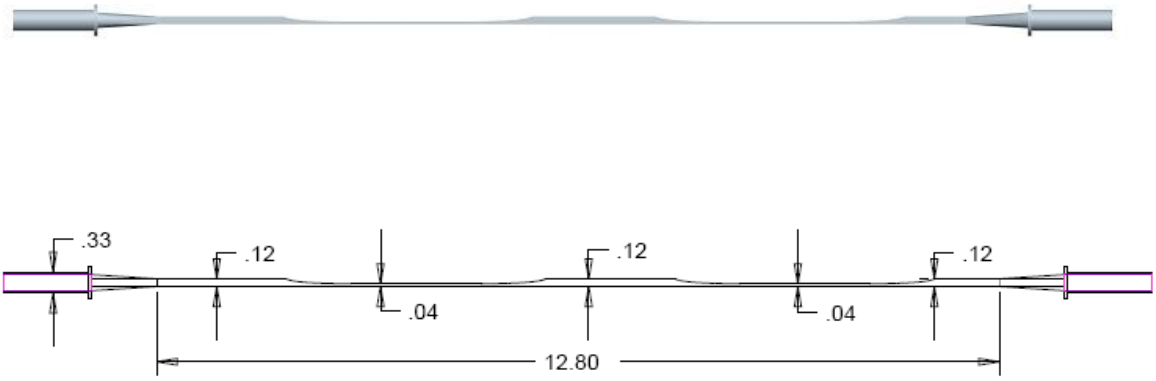

Figure 29. Front view of chamber, which was designed using Pro Engineer. Dimensions are expressed in inches.

2. Manufacturing

The chamber was manufactured by CNC machining at the machine shop of SUNY at Buffalo. The modeled chamber was not manufactured as whole piece, but in two pieces, upper and lower piece, which would work as moulds for the upper and lower section of the final chamber respectively. As seen in Figure 26.

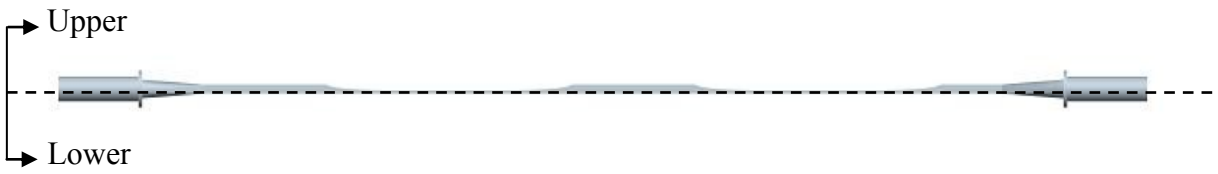

Figure 30. The design was split into two halves, the upper and lower and both halves were manufactured by CNC machining.

The manufactured parts, upper and lower parts were each placed and glued in a box. After it was done, those two boxes were the final moulds for the chamber. A silicone elastomer, Sylgard 184 (Dow Corning), was poured into the moulds and left for 3 days to solidify.

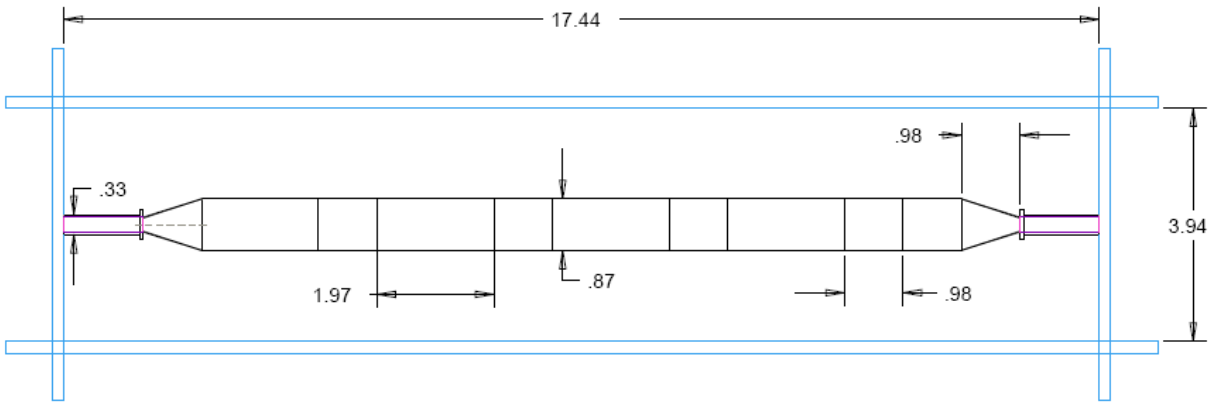

Figure 31. Top view of the mould used for upper section, designed in Pro Engineer. Dimensions are expressed in inches.

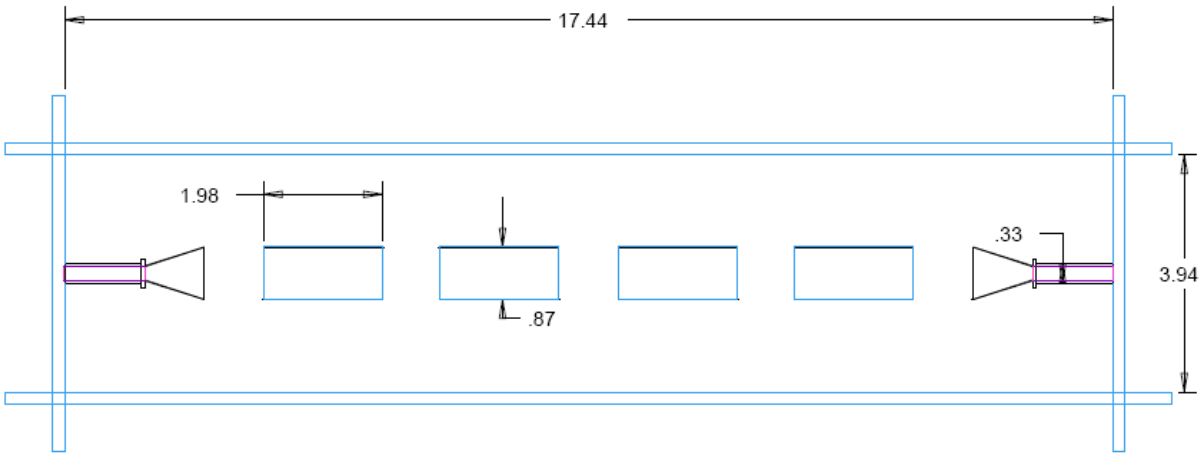

Figure 32. Top view of the mould used for the lower section. Glass coverslips were used in mould for leaving empty groves for the placement of coverslip with the cell monolayer. Designed in Pro Engineer. Dimensions are expressed in inches.

The final two silicone parts, as seen in Figure 31 , were placed together, between two polycarbonate plates, which were bolted to each other, as seen in Figure 32.

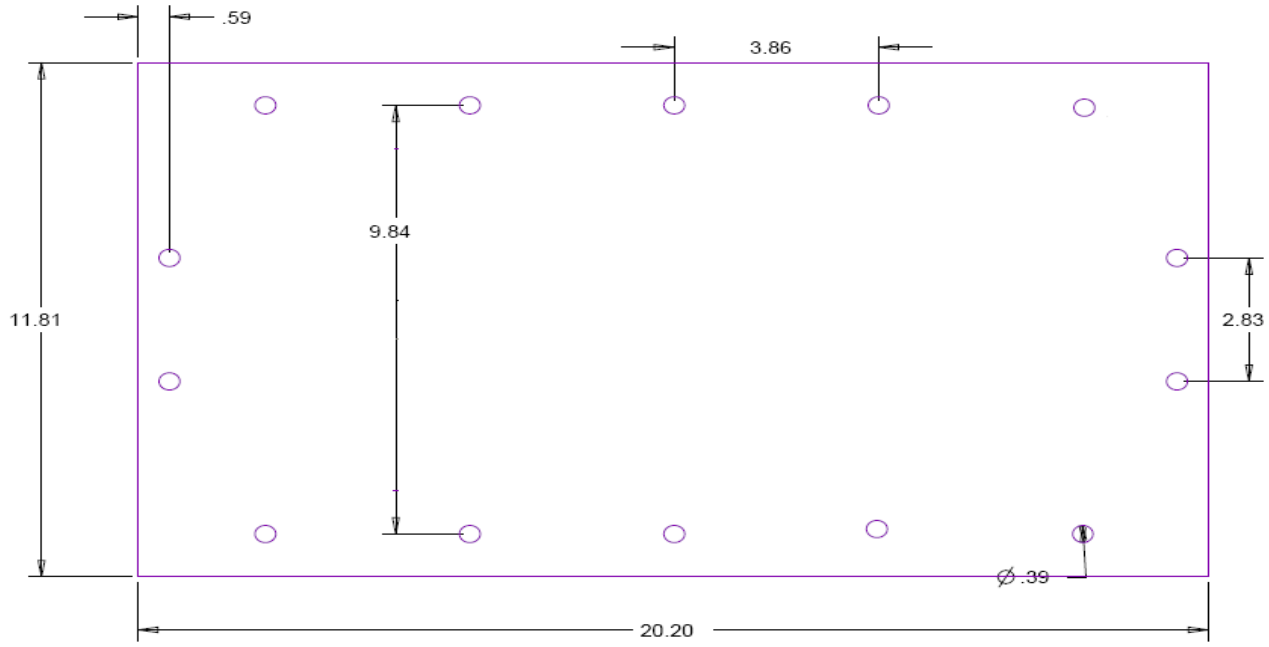

Figure 33. Polycarbonate plates that were used to seal the two silicone parts. Designed in Pro Engineer. Dimensions expressed in inches.

Connectors

The manufactured sections, upper and lower, had groves at both ends to fit connectors, to connect to the tubing. Teflon connectors were designed (Figure 30). The cross section area of the tubing , inlet and outlet were same and simple cylinder connectors were used.

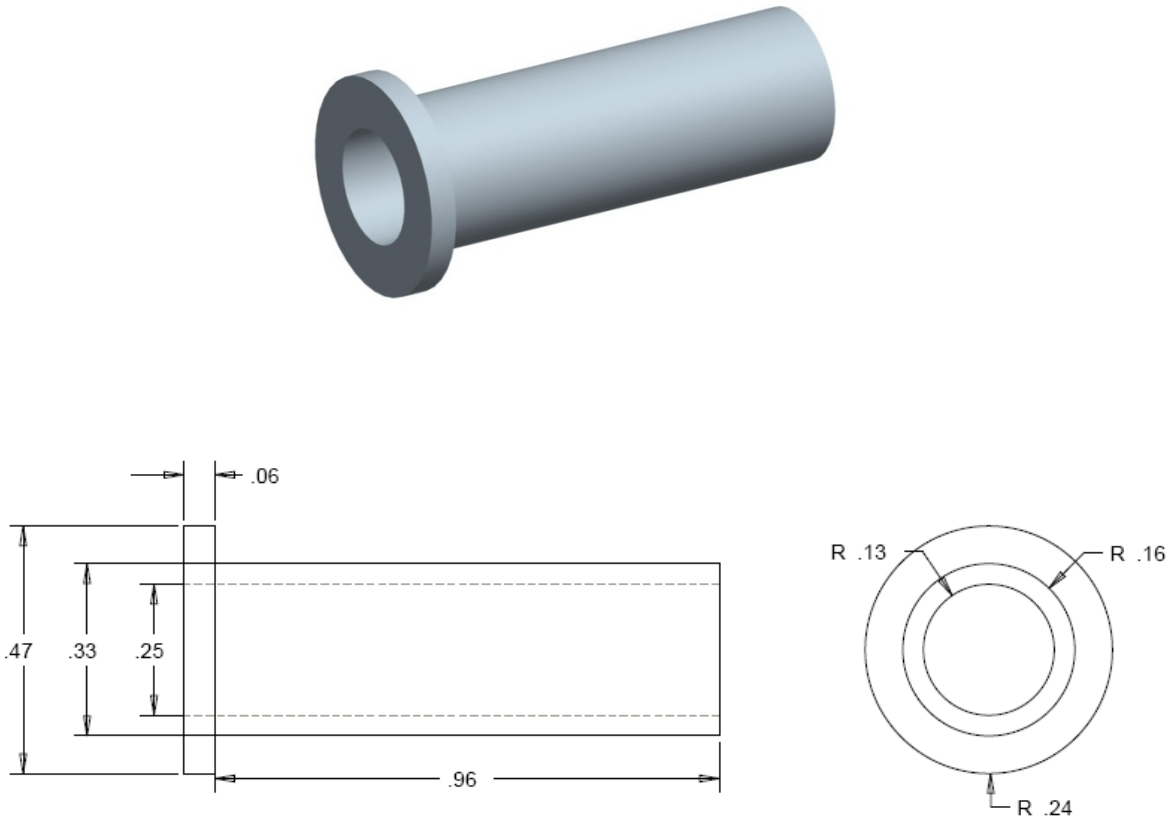

Figure 34. Connector, designed to connect the chamber to tubing. Designed in Pro Engineer.

A.

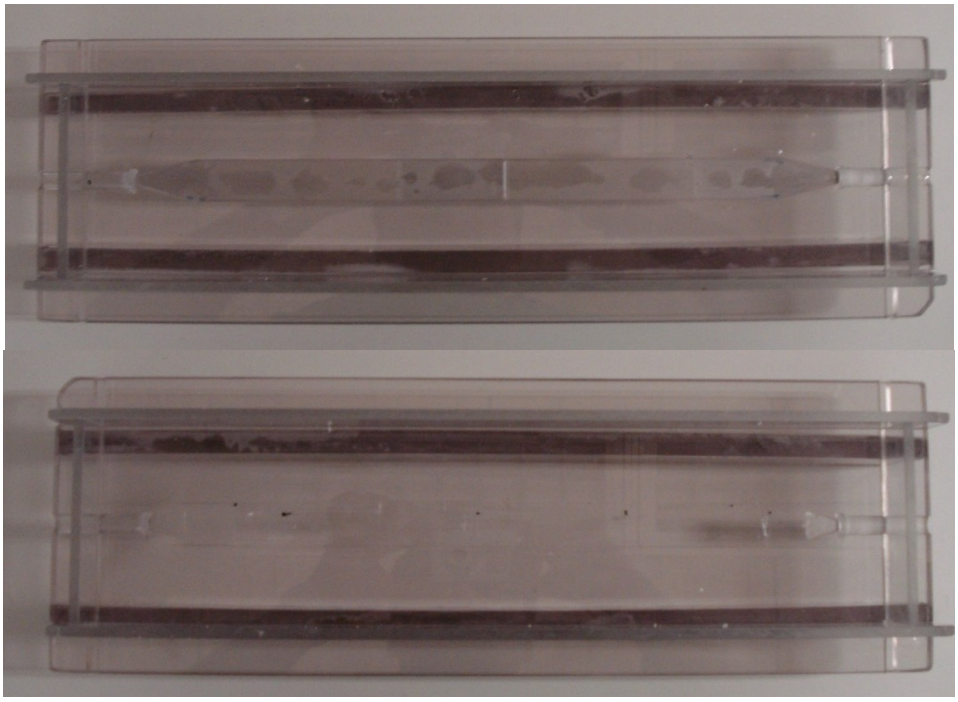

B.

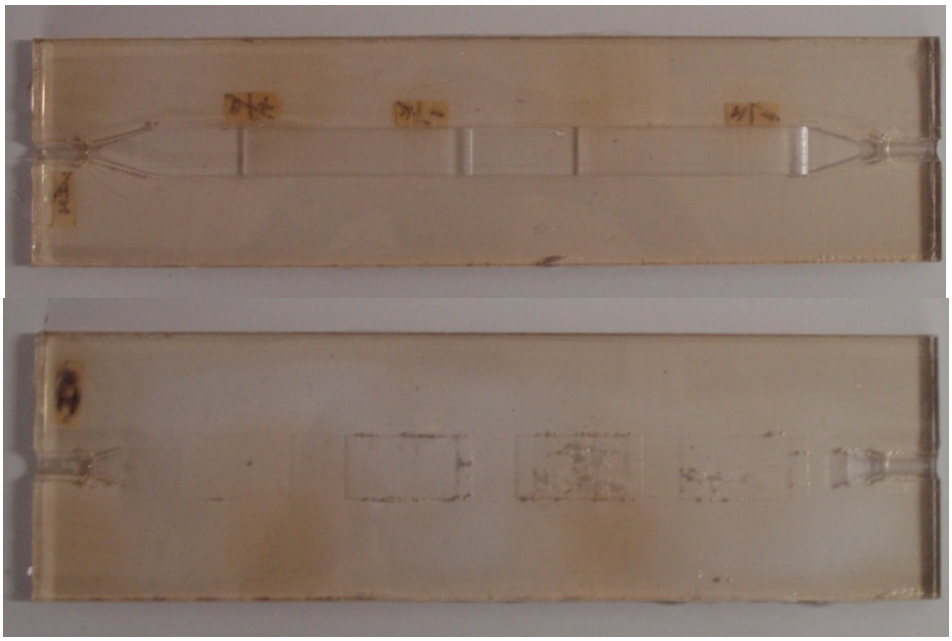

Figure 35. A) Molds used for the upper and lower section of designed chamber. B) Final chamber after the cured silicone elastomer was removed from molds.

3. Recommended Materials

Stainless steel: Biocompatible, autoclavable, strong, difficult to manufacture (expensive/time consuming machining). All stainless steels must be of the same grade (18/10, 18/8, etc.) as leaching of chromium-3 (accelerated by dissimilar metals) can be toxic to cells

Polycarbonate: biocompatible, autoclavable, raw materials and manufacturing are much cheaper than stainless steel, but still relatively expensive as a polymer. Material is strong but will fracture under stress during autoclaving

Silicone: biocompatible, autoclavable, can be molded into complex surfaces, distensible, provides good seal against other materials, strong, transparent (depending on formulation), requires molding/set time

Teflon: biocompatible, autoclavable, can be easily machined, relatively expensive polymer

Acrylic: NOT autoclavable (will distort/melt)

4. Reynolds number

Density: $\rho = 1.02 \times 10^3 kg / m^3$

Dynamic viscosity: $\mu = 3.5cP = 0.0035 Ns / m^2$

Flow rate: $Q = 2000ml / \min = 0.033 \times 10^{-3} m^3 / \sec$

Reynolds number: $\mathrm{Re}_x = \frac{\rho u_x D_x}{\mu}$

Where D_x is the hydraulic diameter of the rectangular cross section area at each x-position and is given by:

$$D_x = \frac{2.w.h_x}{w + h_x}$$

$$\Rightarrow \quad \mathrm{Re}_x = \frac{2\rho u_x w h_x}{\mu(w + h_x)}$$

$$\Rightarrow \quad \mathrm{Re}_x = \frac{2\rho Q}{\mu(w + h_x)}$$

$$\text{where} \quad h_x = \frac{h_o}{\sqrt{1 + \frac{w h_o^2}{6\mu Q}\frac{\partial \tau}{\partial x} x}}.$$

Substituting the values, and plotting Re against distance in converging section we get the following plot. The Re variation in the diverging section is identical in the opposite direction.

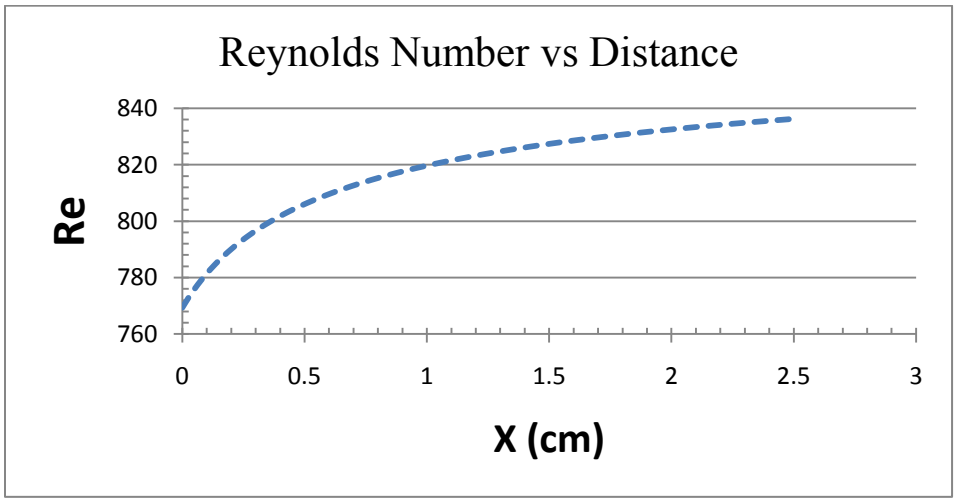

Figure 36. Reynolds number in the converging section

Appendix B: Notes on Flow Loop Development

1. Sterilization:

The most common and rather difficult aspect of the in vitro techniques is the requirement to carry out various operations under aseptic conditions.

a) Steam Autoclave

Steam autoclaving is a method of sterilizing with water vapor under high pressure. Nearly all microbes are killed on exposure to the superheated steam of an autoclave. Normally, glassware, cotton plugs, gauze, plastic caps, filters or pipettes are autoclaved at 121^{o}C and 15 psi for 20-30 min. For all the components to be able to undergo steam autoclave, materials should be able to withstand at least one hour at 120^{o} C temperature for repeated cycles. It is important to have a "fully-autoclavable loop", as components can be autoclaved together, thus limiting possible contamination during transfer/assembly. Fatigue could cause leakage over time, even though some materials will not melt. Most materials will expand and contract during heating/cooling, causing stress fractures in rigid materials or gap formation between stressed materials such as around tightened threaded fittings (pipe fittings - NPT).

b) Hot Dry Air

Glass wares, metal instruments and aluminum foil can be sterilized by exposure to hot dry air (160^{o}C - 180^{o}C) for 2-4 hr. in a hot- air oven. All items should be properly sealed before sterilizing.

c) Flame Sterilization

Metallic instruments like forceps, scalpels, needles and spatulas are sterilized by dipping in 95% ethanol, followed by flaming and cooling. This technique is called flame sterilization. Autoclaving of metallic instruments is generally avoided as they may rust and become blunt. Components cleaned with ethanol are technically not sterile. The only advantage of using ethanol for sterilization is the freedom to use a large variety of materials for construction. We have not been able to achieve "adequate sterilization" using this method.

d) Formalin Gas

This method is less effective in complex devices where the gas cannot access crevices or tight spots. This method can be used though it is difficult to achieve complete sterilization.

e) Ionizing Radiation

This method can be effective if the radiation can reach everywhere. We have not tested this method for our devices.

2. Maintaining ideal conditions (temperature, humidity, and pH) :

a) Biological Safety Cabinets

Most cell culture handling is now carried out in Class II Biological safety cabinets. These cabinets maintain a clean working environment for cell handling and help to provide protection to the operator and environment. Horizontal laminar flow cabinets are useful for media preparation but are not desirable for cell culture work due to the risk of possible contaminants in the cell culture being blown into the face of the operator. The effectiveness of a BSC is

dependent on its position, correct use, regular testing and maintenance. Cabinets should be sited away from doors and through-traffic. Movement in the area of a BSC will disturb airflow and so access to the area should be restricted to essential personnel. When working within a BSC it is important to minimize the potential for contamination of the working environment and cross-contamination between cell lines. Bunsen or similar burner should not be used inside a BSC (unless absolutely required for a specialized procedure) as they disrupt the airflow pattern, can damage the HEPA filters and pose a fire risk.

b) Incubators

Cell cultures require a strictly controlled environment in which to grow. Specialist incubators are used routinely to provide the correct growth conditions, such as temperature, degree of humidity and CO_2 levels in a controlled and stable manner. Generally they can be set to run at temperatures in the range 28ºC (for insect cell lines) to 37ºC (for mammalian cell lines) and set to provide CO_2 at the required level (e.g. 5-10%). Some incubators also have the facility to control the O_2 levels. Copper-coated incubators are also now available. These are reported to reduce the risk of microbial contamination within the incubator due to the microbial inhibitory activity of copper. For our experiments, it is ideal to keep a majority of the loop in a 37°C, 5% CO_2 tissue culture incubator. Assuming the use of appropriate media buffers, a syringe filter can be used to vent the media reservoir to the air in the incubator; this will stabilize the pH at 7.2-7.4. The temperature is relatively stable.

c) Water Bath

A water bath uses water to heat or maintain a constant temperature of laboratory materials or equipment. Even though a water bath can help to maintain the temperature of the loop at 37°, but evaporation from the water bath and heat exchange from the non-submersed parts of the loop, cause temperature instability and make the process difficult.

4. Experimental substrate:

Cover slip/Cover glass (Fisher Scientific, VWR) can be used as cells will remain confluent at WSSs in excess of 200 dynes/cm2. Microscope slides do not hold cells under high WSS. Thermanox™ polymer slides do not work well with fluorescent staining.

5. Tubing:

a) Pump tubing

It is important to select tubing with appropriate chemical resistance towards the liquid being pumped. Material should be biocompatible and autoclavable. Due to high flow rate high-performance (thicker-walled), low spallation tubing is ideal. Spallation causes contamination and other side effects. Worn tubing does not fully recover after compression, causing the flow rate to decrease over time. Using larger ID tubing will decrease the stroke volume of the pump, allowing lower rpms to be used which lowers tubing wear. Types of tubing commonly used in peristaltic pumps include Polyvinyl chloride (PVC),Silicone rubber and Fluoropolymer.

b) Loop tubing

In addition to its use as a part of a peristaltic pump flexible tubing also required for the rest of the loop. Though it need not be thick walled or spallation free, it should be autoclavable and biocompatible. Cheaper and smaller I.D. tubing can be used.

Tygon®: biocompatible, autoclavable, broad chemical resistance, cheap, but discolors on autoclaving and distorts under stress in the autoclave, leading to leakage.

Silastic® (silicone): translucent, autoclavable, biocompatible, cheap and very low leakage

Flexelene® : autoclavable, animal derivative free, biocompatible

c) Connectors:

Connectors should be biocompatible and autoclavable (polycarbonate, Teflon), though some non-autoclavable materials are cheaper and have long life under repeated autoclaving (Nylon).

6. Pump:

A pump that does not come in contact with the fluid is ideal for in vitro studies. A peristaltic or tubing pump fits this criterion. The main advantages are

a) Non contamination

The peristaltic pump creates a contamination-free pumping system. The fluid being pumped remains inside the tubing at all times and thus never comes in contact with any pump gears, seals, diaphragms, or other moving parts. As a result, finding a pump compatible with a particular solution is as simple as choosing a chemically compatible tubing.

b) Simple operation

Peristaltic pumps are simple to operate and easy to customize. They are self-priming, and many models have interchangeable pump heads that can be mounted in minutes using finger-tightened screws. Engineering advances have yielded designs that allow the tubing even in large process pumps to be loaded or replaced in seconds.

c) Low maintenance

Peristaltic pumps require very little maintenance beyond tubing replacement. Tubing must be replaced periodically to offset reduced flow performance. This procedure typically takes just seconds, which can be an advantage when using the same pump to transfer or dispense different chemicals. When solutions are changed, only the tubing needs to be changed, and the pump can be up and running within minutes.

d) Tubing materials

Peristaltic pump systems are compatible with a wide range of tubing materials, including silicone, thermoplastics, Viton, and even rigid PTFE.

Peristaltic pumps are ideal for low flow rates, as high flow rates cause wear of pump tubing, though this can be take care of to some extent by increasing the tubing size and thus reducing the rpms.

Though advanced pumps are available, it is preferred to avoid pumps that come into contact with the fluid.

7. Reservoir:

Reservoir should be autoclavable and biocompatible. Venting a media reservoir to the air in the incubator via a syringe filter will stabilize the pH at 7.2-7.4. Thus a rubber stopper with three holes (inlet, outlet, air filter) for silicone tubing is recommended because it is autoclavable, cheap and can be placed in a variety of different sized glass media bottles.

8. Preventing Leakage:

For sealing cracks, silicone caulk is recommended as it provides a good seal , relatively quick drying, can be autoclaved repeatedly and is also cheap.

9. Flow Rate Measurement:

Flow rate measurement is important to maintain a constant flow rate. Following are the recommended flow meters:

Ultrasonic Flow Probes: contamination free measurement of flow, no leak potential, allows for easy installation without disturbing existing flow loop, can be calibrated to tubing and media, but pipe material must be compatible with ultrasonic sensor, requires sufficient knowledge of the flow and media and are very expensive. Transonic Flow Probe (Transonic Systems, ME6PXL436) is currently calibrated for .25" ID x .375" OD Silastic tubing (Cole-Parmer cat# 515-015) and media containing: DMEM, 8%Dextran, 5% FBS. The sensor clamps onto flexible tubing and measures flow rate inside.

Other references : [43], [33]

Appendix C: *In Vitro* Results

Results shown in the Chapter 4, are only from one experiment (Ex 3) out of total three experiments. The same results from the other two experiments are listed below.

Experiment 2

Baseline WSS≈ 35 dyn/cm^2

A.

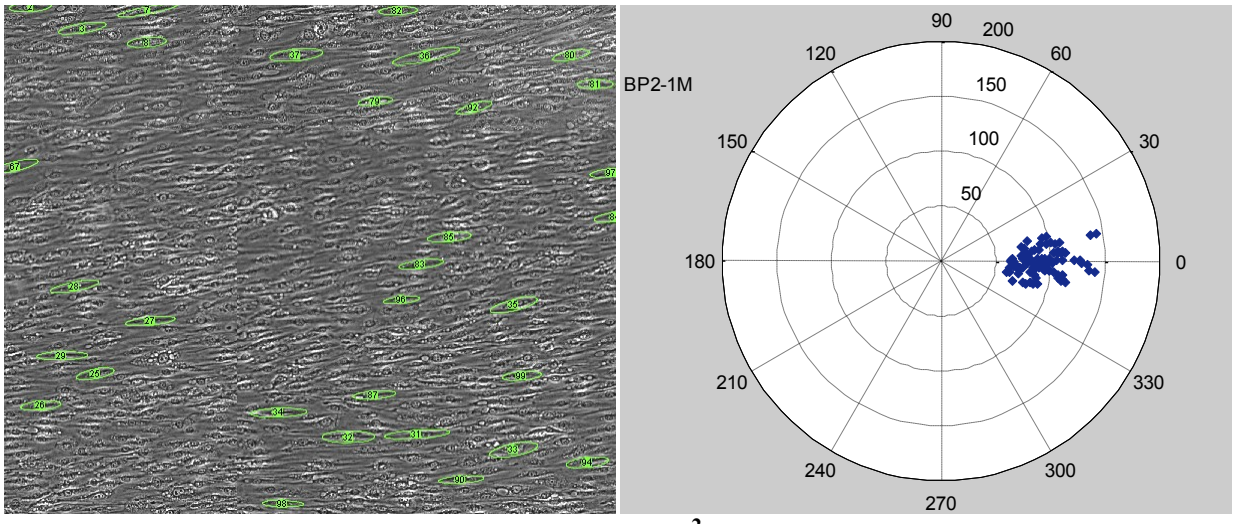

WSS≈ 35 dyn/cm^2

B.

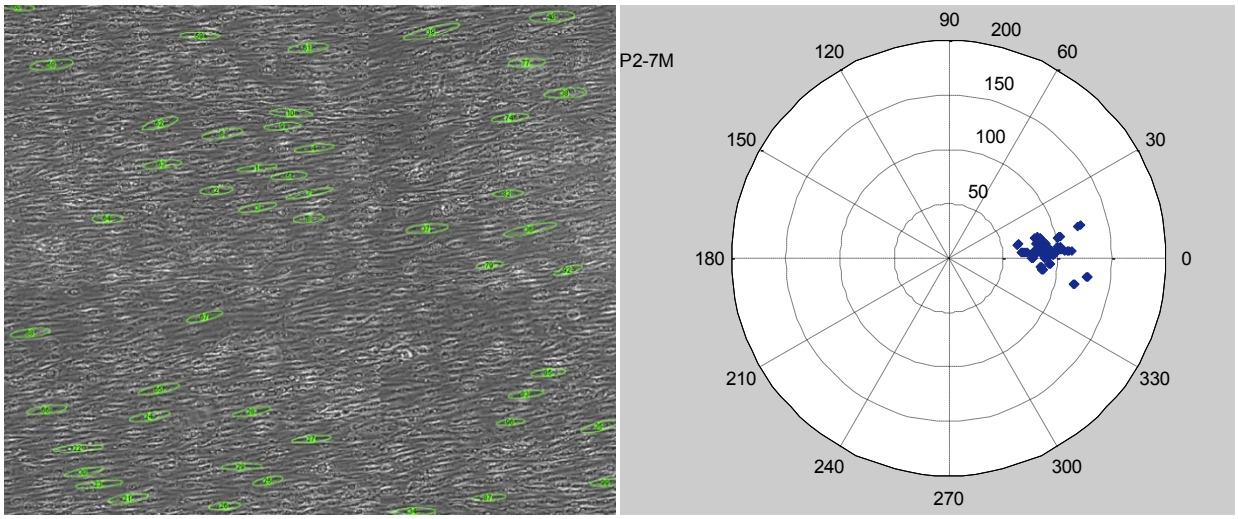

WSS≈ 35 dyn/cm^2

POSITIVE WSSG

C.

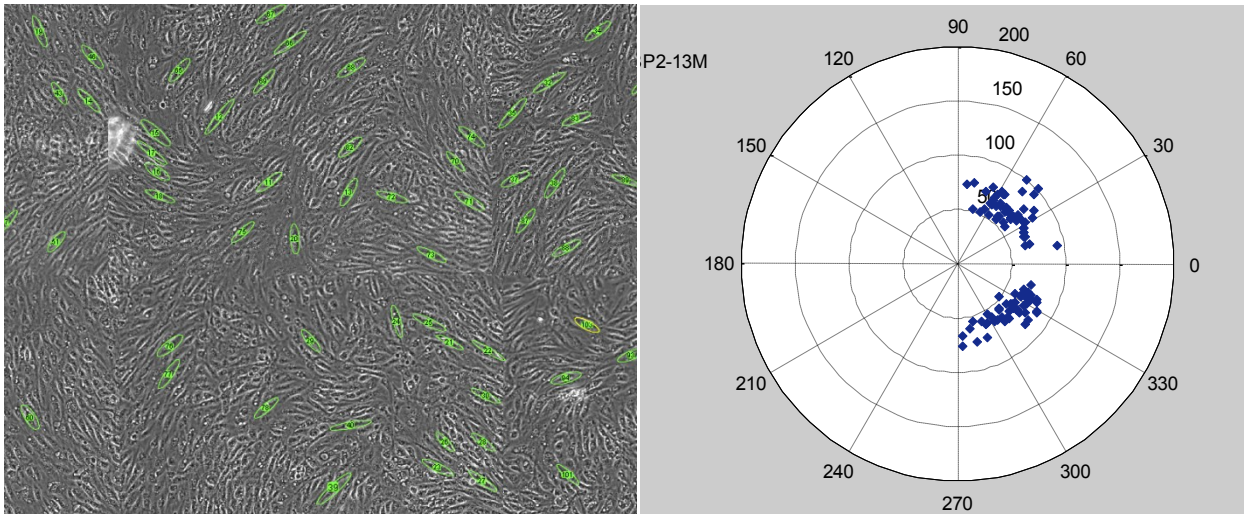

WSS≈ 170-220 dyn/cm^2

D.

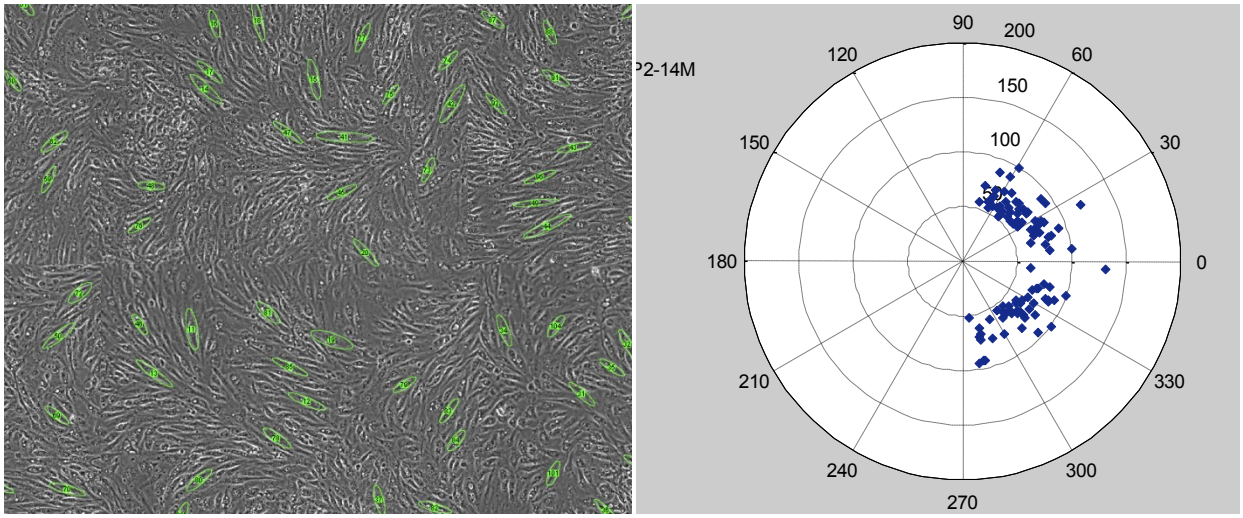

WSS≈ 200-226 dyn/cm^2

E.

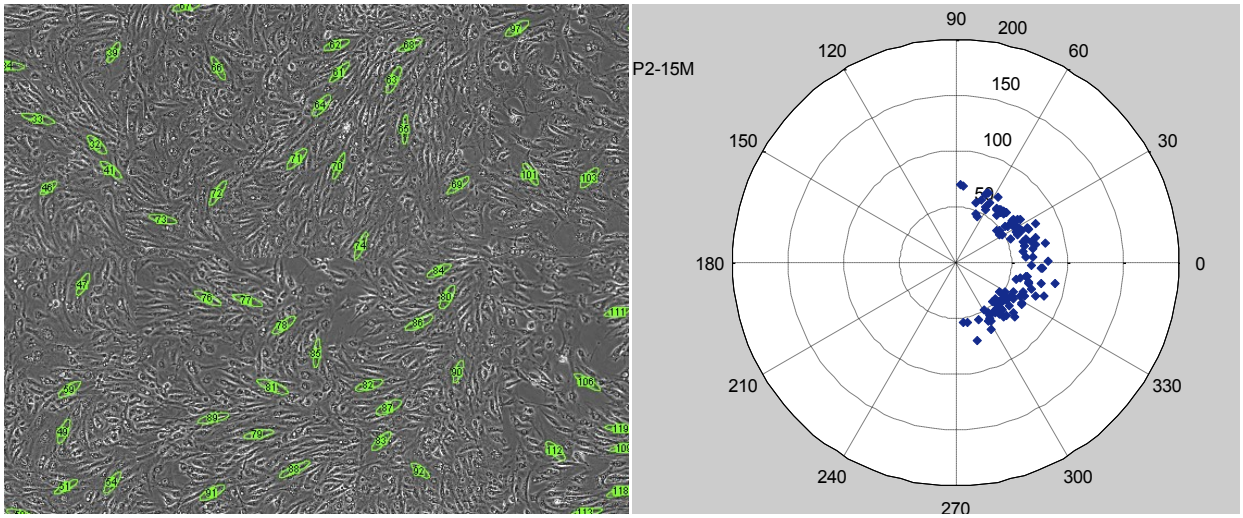

WSS≈ 226-260 dyn/cm^2

High WSS≈285 dyn/cm^2

A.

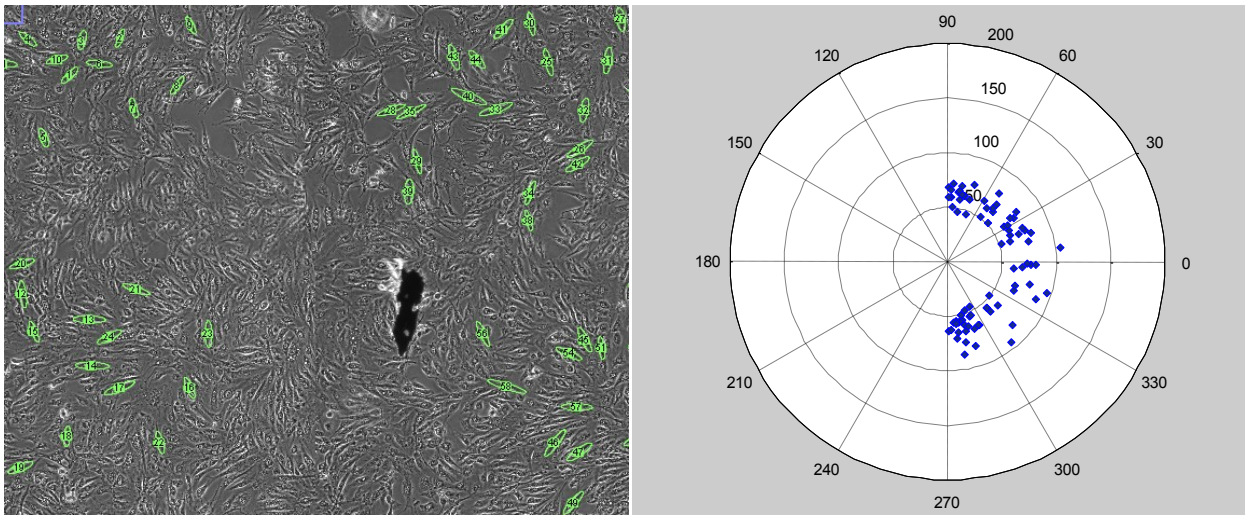

WSS≈ 285 dyn/cm^2

B.

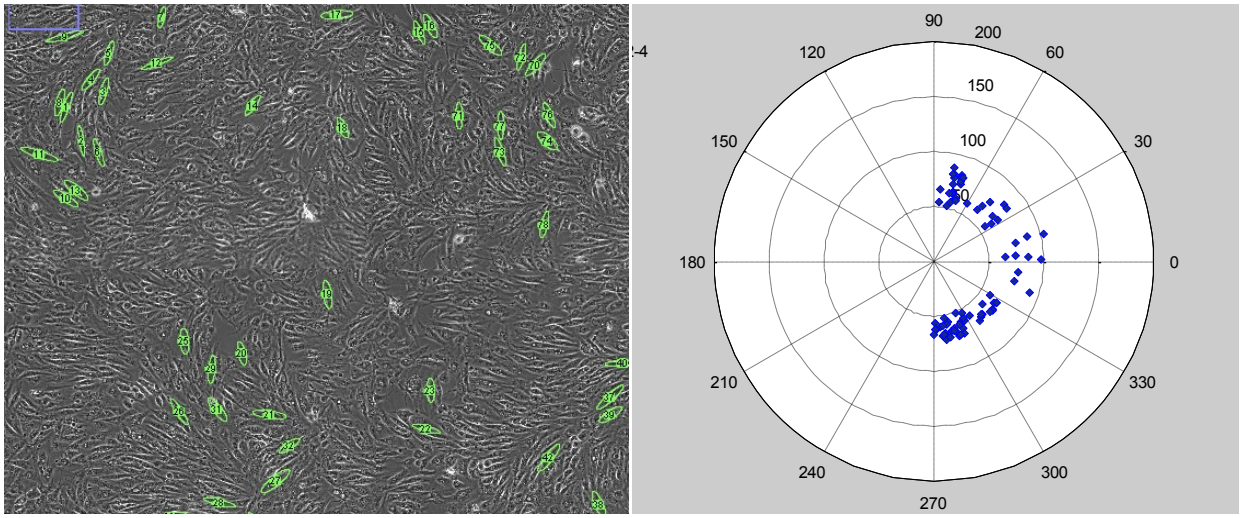

WSS≈ 285 dyn/cm^2

Negative WSSG

C.

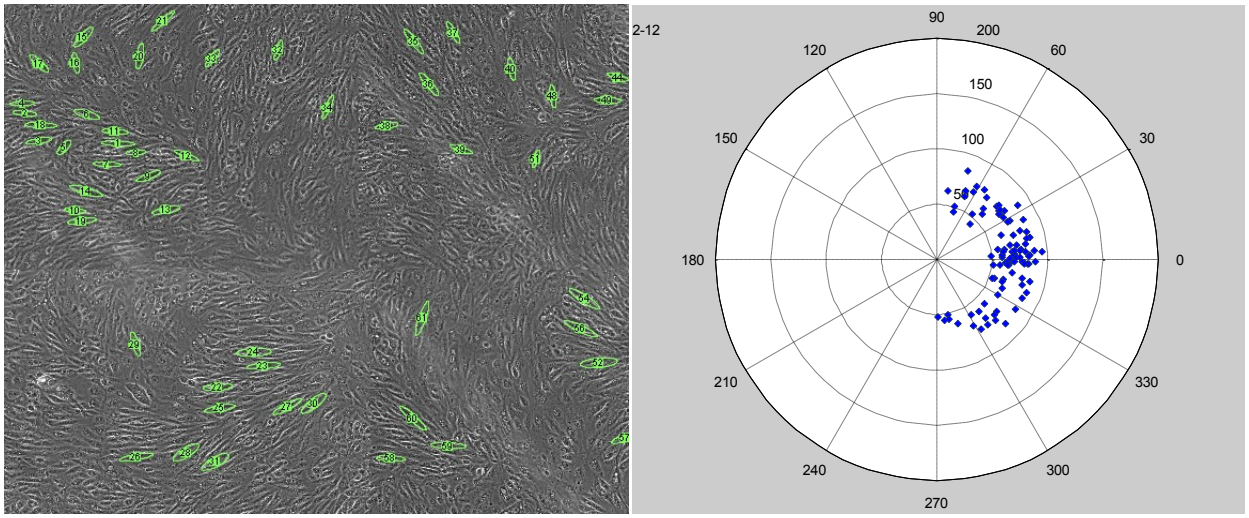

WSS≈ 180-146 dyn/cm^2

D.

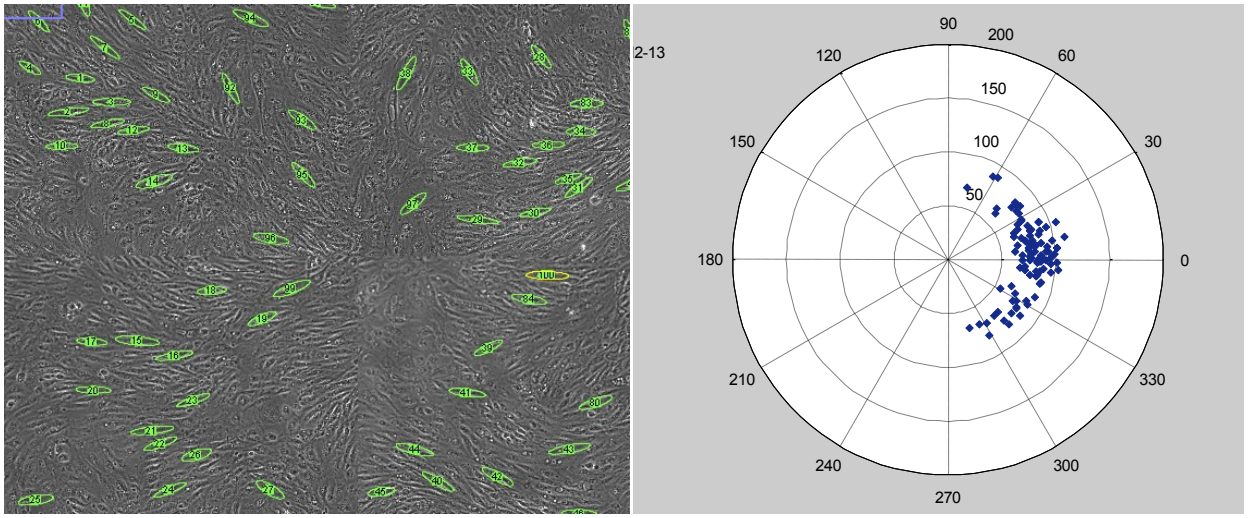

WSS≈ 146-110 dyn/cm^2

E.

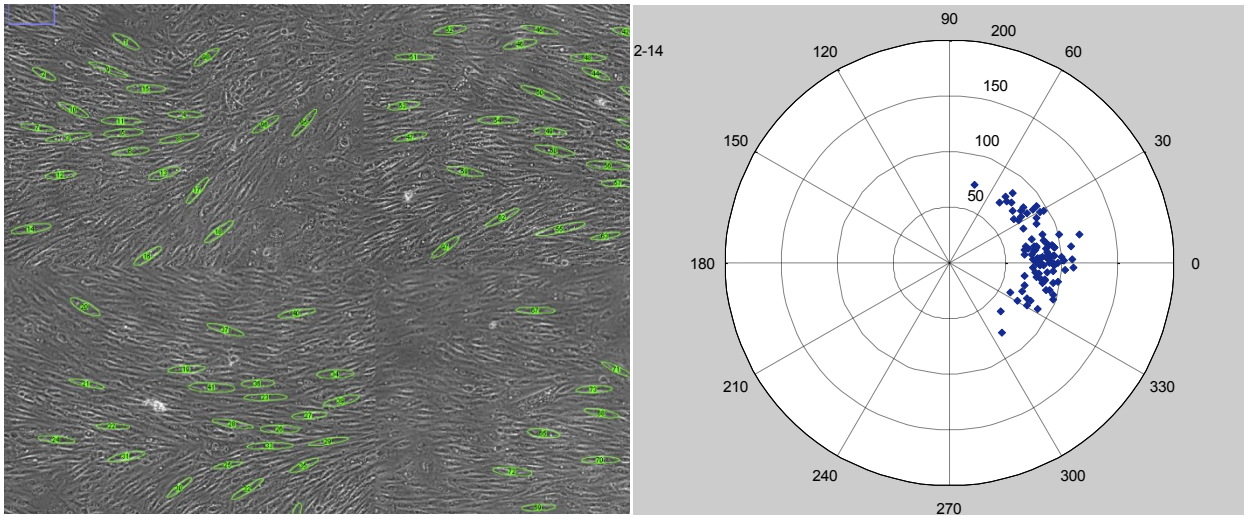

WSS≈ 110-80 dyn/cm^2

EXPERIMENT 1

Baseline WSS≈ 35 dyn/cm^2

A.

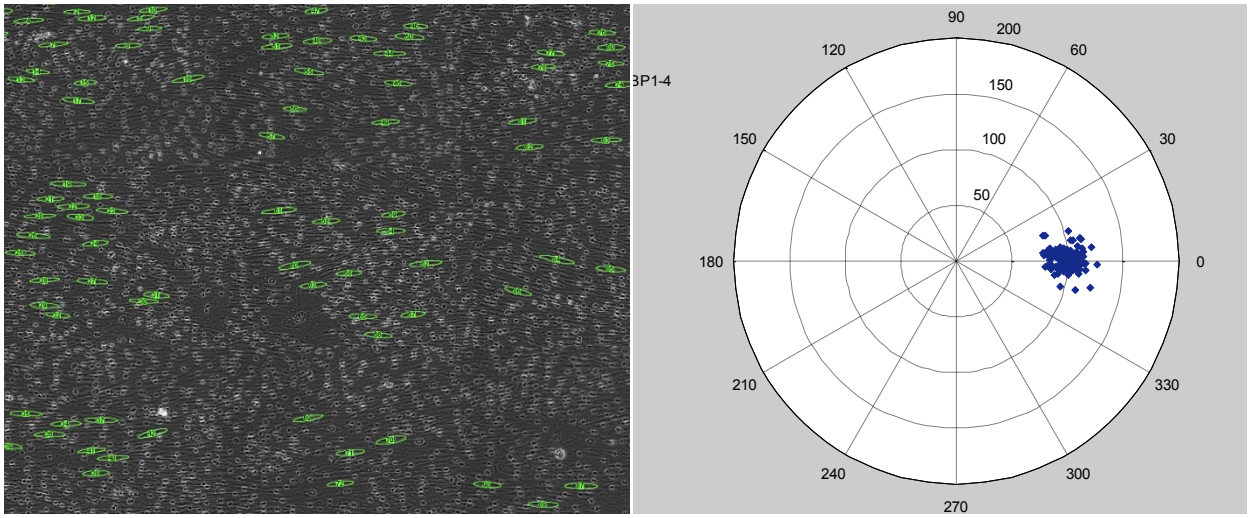

WSS≈ 35 dyn/cm^2

B.

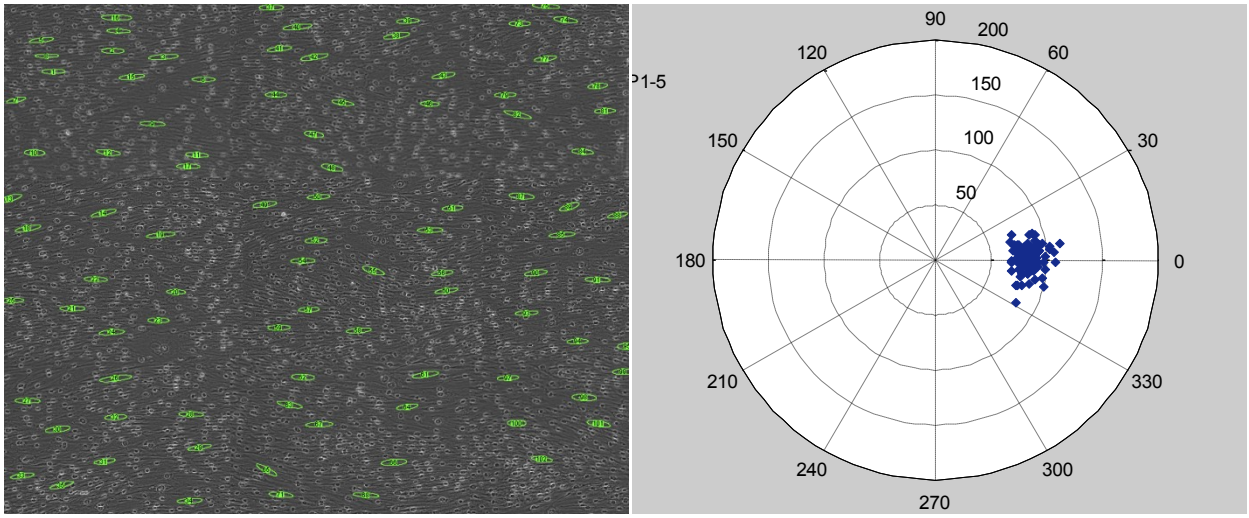

WSS≈ 35 dyn/cm^2

POSITIVE WSSG

C.

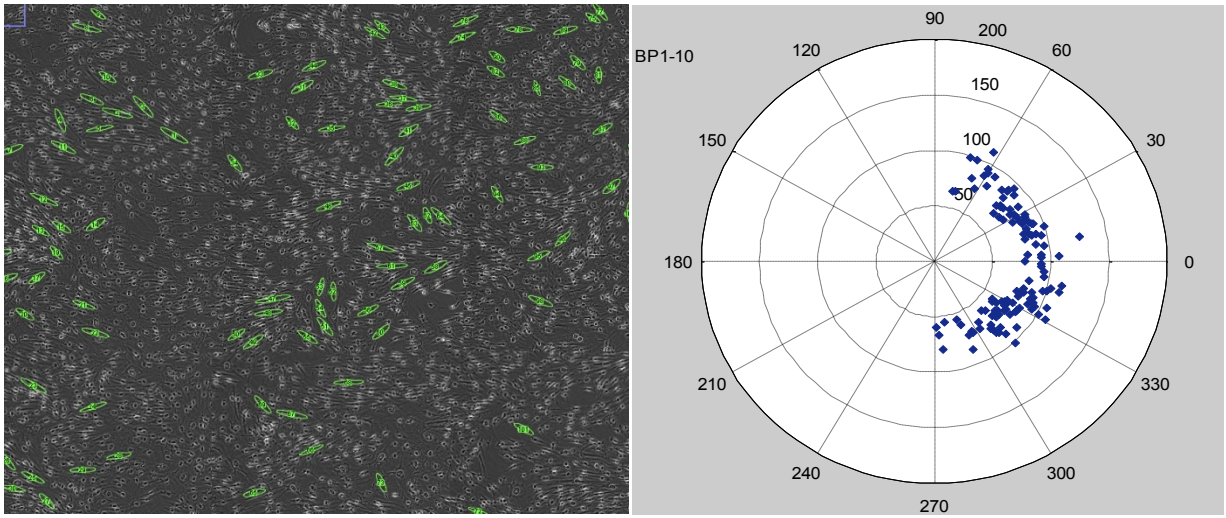

WSS≈ 134-167 dyn/cm^2

D.

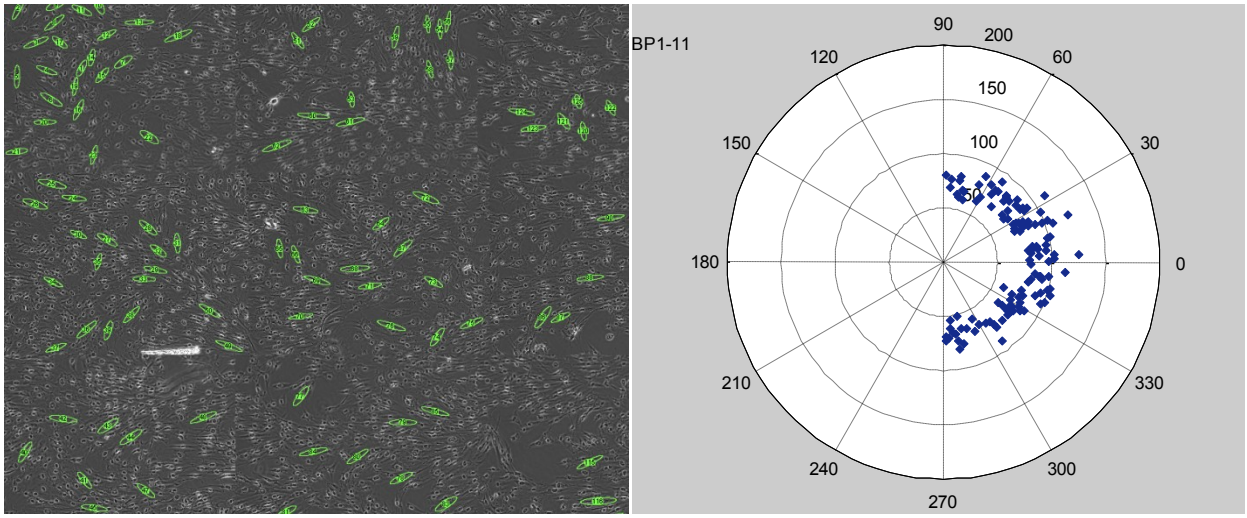

WSS≈ 167-200 dyn/cm^2

E.

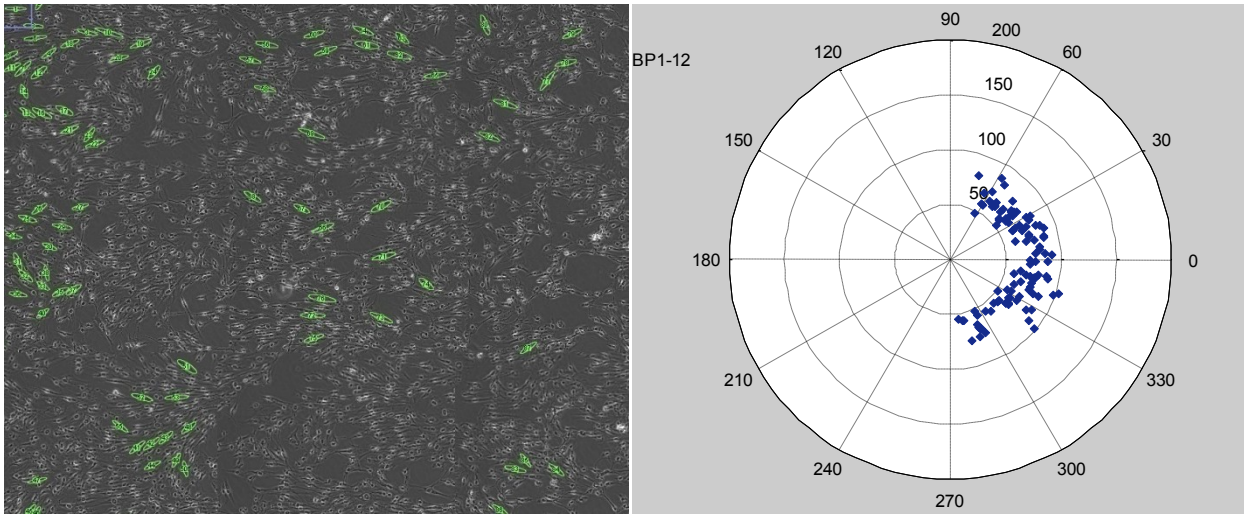

WSS≈ 200-230 dyn/cm^2

High WSS≈285 dyn/cm^2

A.

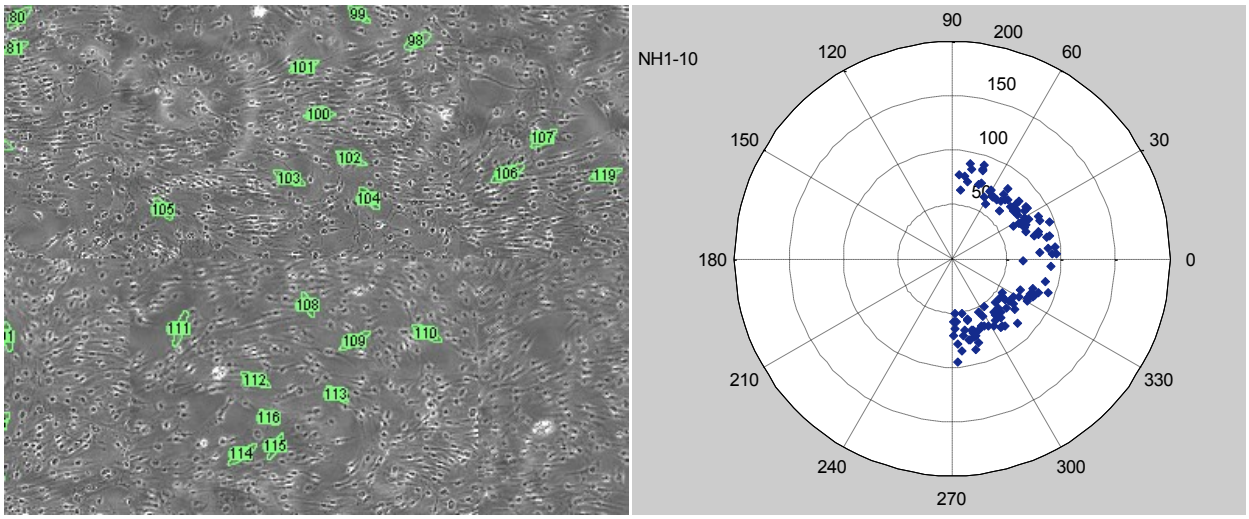

WSS≈ 285 dyn/cm^2

B.

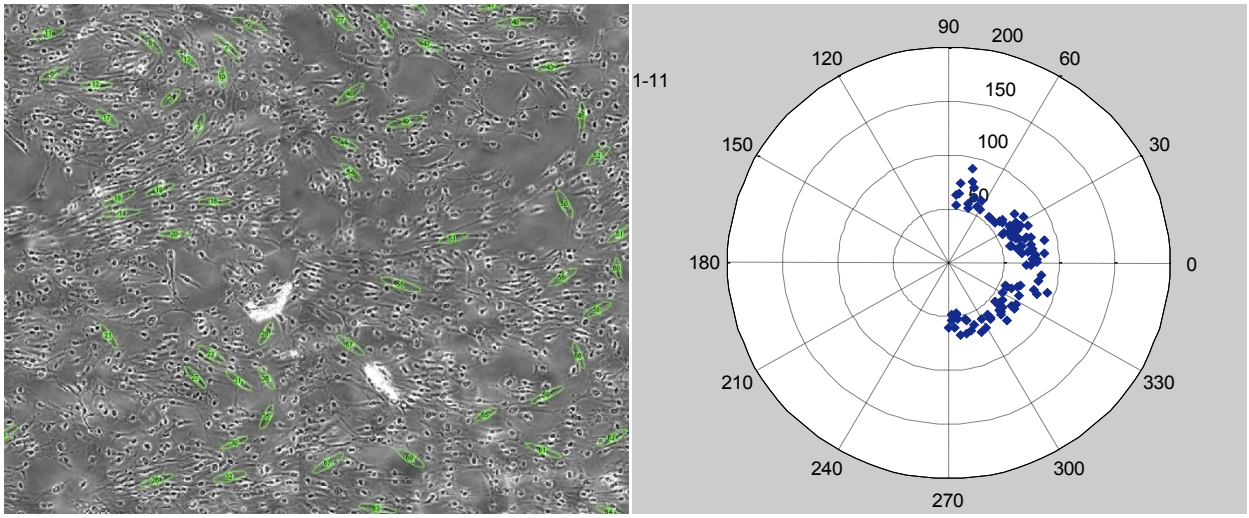

WSS≈ 285 dyn/cm^2

NEGATIVE WSSG

C.

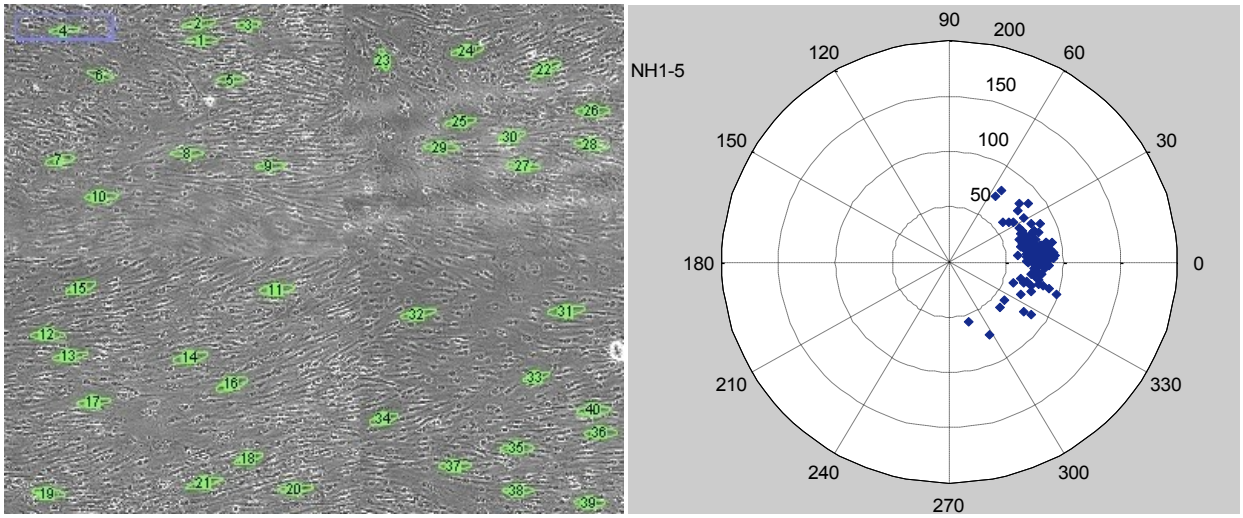

WSS≈ 196-142 dyn/cm^2

D.

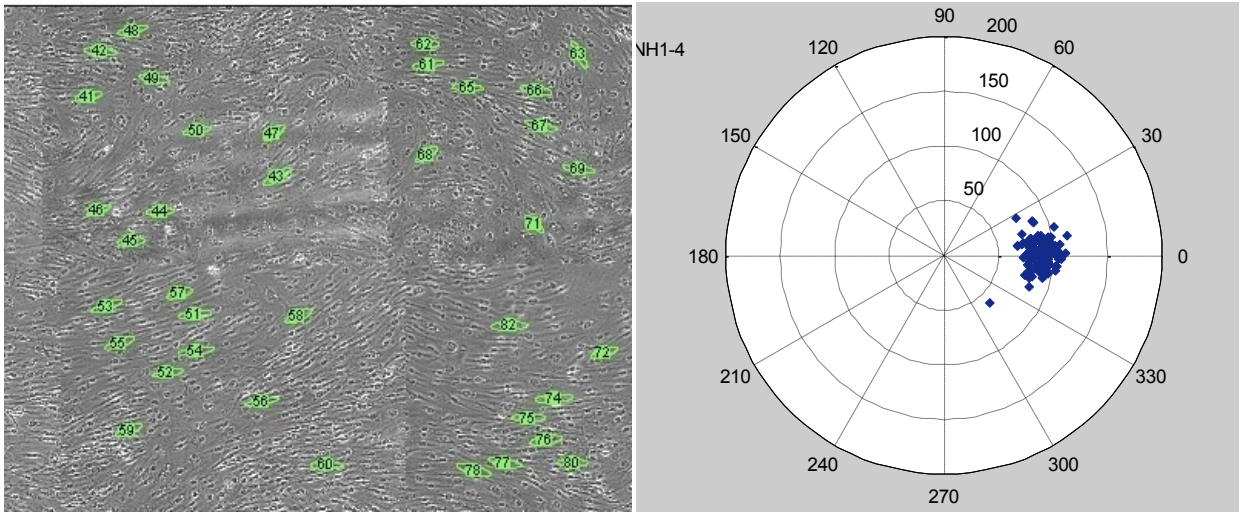

WSS≈142-86 dyn/cm^2

E.

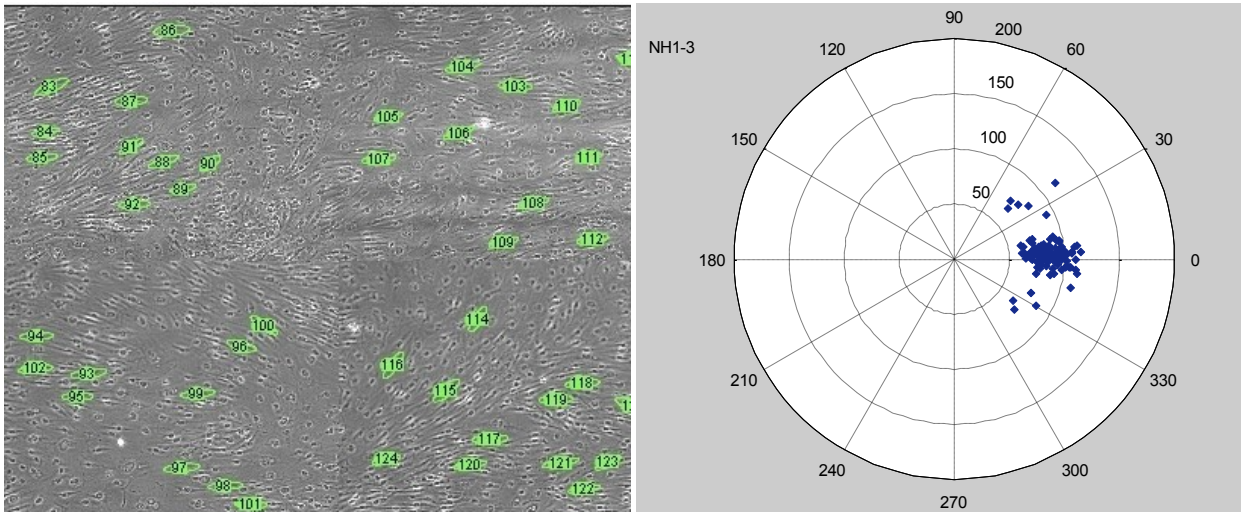

WSS≈ 86-33 dyn/cm^2

References

1. Schievink, W.I., et al., *Sudden death from aneurysmal subarachnoid hemorrhage.* Neurology, 1995. **45**(5): p. 871-4.
2. Phillips, L.H., 2nd, et al., *The unchanging pattern of subarachnoid hemorrhage in a community.* Neurology, 1980. **30**(10): p. 1034-40.
3. Sacco, R.L., et al., *Subarachnoid and intracerebral hemorrhage: natural history, prognosis, and precursive factors in the Framingham Study.* Neurology, 1984. **34**(7): p. 847-54.
4. Longstreth, W.T., Jr., et al., *Clinical course of spontaneous subarachnoid hemorrhage: a population-based study in King County, Washington.* Neurology, 1993. **43**(4): p. 712-8.
5. Fogelholm, R., J. Hernesniemi, and M. Vapalahti, *Impact of early surgery on outcome after aneurysmal subarachnoid hemorrhage. A population-based study.* Stroke, 1993. **24**(11): p. 1649-54.
6. Inagawa, T., et al., *Study of aneurysmal subarachnoid hemorrhage in Izumo City, Japan.* Stroke, 1995. **26**(5): p. 761-6.
7. Schievink, W.I., *Intracranial aneurysms.* N Engl J Med, 1997. **336**(1): p. 28-40.
8. Hop, J.W., et al., *Case-fatality rates and functional outcome after subarachnoid hemorrhage: a systematic review.* Stroke, 1997. **28**(3): p. 660-4.
9. Brisman, J.L., J.K. Song, and D.W. Newell, *Cerebral aneurysms.* N Engl J Med, 2006. **355**(9): p. 928-39.
10. Forget, T.R., Jr., et al., *A review of size and location of ruptured intracranial aneurysms.* Neurosurgery, 2001. **49**(6): p. 1322-5; discussion 1325-6.

11. Ohashi, Y., et al., *Size of cerebral aneurysms and related factors in patients with subarachnoid hemorrhage.* Surg Neurol, 2004. **61**(3): p. 239-45; discussion 245-7.

12. Britz, G.W., et al., *Impact of surgical clipping on survival in unruptured and ruptured cerebral aneurysms: a population-based study.* Stroke, 2004. **35**(6): p. 1399-403.

13. Olafsson, E., W.A. Hauser, and G. Gudmundsson, *A population-based study of prognosis of ruptured cerebral aneurysm: mortality and recurrence of subarachnoid hemorrhage.* Neurology, 1997. **48**(5): p. 1191-5.

14. Meng, H., et al., *A model system for mapping vascular responses to complex hemodynamics at arterial bifurcations in vivo.* Neurosurgery, 2006. **59**(5): p. 1094-100; discussion 1100-1.

15. Meng, H., et al., *Complex Hemodynamics at the Apex of an Arterial Bifurcation Induces Vascular Remodeling Resembling Cerebral Aneurysm Initiation.* Stoke, 2007 (accepted).

16. Krex, D., H.K. Schackert, and G. Schackert, *Genesis of cerebral aneurysms--an update.* Acta Neurochir (Wien), 2001. **143**(5): p. 429-48; discussion 448-9.

17. Sekhar, L.N. and R.C. Heros, *Origin, growth, and rupture of saccular aneurysms: a review.* Neurosurgery, 1981. **8**(2): p. 248-60.

18. Karino, T., M. Montomiya, and H.L. Goldsmith, *Flow Patterns in Model and Natural Branching vessels.* . In: Fluid Dynamics as a Localizing Factors for Atherosclerosos, 1983: p. 66-83.

19. Dewey, C.F., *In: Dynamics of Arterial Flow.* Adv Exp Med Biol, 1979. **115**: p. 55.

20. Friedman, M.H., et al., *Hemodynamic measurements in human arterial casts, and their correlation with histology and luminal area.* J Biomech Eng, 1980. **102**(3): p. 247.

21. Deng, D.X., et al., *Differences in vascular bed disease susceptibility reflect differences in gene expression response to atherogenic stimuli.* Circ Res, 2006. **98**(2): p. 200-8.

22. Ku, D.N. and D.P. Giddens, *Pulsatile flow in a model carotid bifurcation.* Arteriosclerosis, 1983. **3**(1): p. 31-9.

23. Ku, D.N. and D. Liepsch, *The effects of non-Newtonian viscoelasticity and wall elasticity on flow at a 90 degrees bifurcation.* Biorheology, 1986. **23**(4): p. 359-70.

24. Richardson, P.D., *Blood Flow, Pressure and Wall Stresses Near Arterial Branches.* Abstracts of the First World Congress of Biomechanics, 1990. **2**: p. 332.

25. Davis, P.H., *Effects of Non-newtonian Fluid Behavior on Wall Shear in a Separated Flow Region.* Abstracts fo the First World Congress of Biomechanics, 1990. **2**: p. 301.

26. Zarins, C.K., et al., *Carotid bifurcation atherosclerosis. Quantitative correlation of plaque localization with flow velocity profiles and wall shear stress.* Circ Res, 1983. **53**(4): p. 502-14.

27. Davies, P.F., *Flow-mediated endothelial mechanotransduction.* Physiol Rev, 1995. **75**(3): p. 519-60.

28. Langille, B.L. and F. O'Donnell, *Reductions in arterial diameter produced by chronic decreases in blood flow are endothelium-dependent.* Science, 1986. **231**(4736): p. 405-7.

29. Pohl, U., et al., *Crucial role of endothelium in the vasodilator response to increased flow in vivo.* Hypertension, 1986. **8**(1): p. 37-44.

30. Flaherty, J.T., et al., *Endothelial nuclear patterns in the canine arterial tree with particular reference to hemodynamic events.* Circ Res, 1972. **30**(1): p. 23-33.

31. Remuzzi, A., et al., *Orientation of endothelial cells in shear fields in vitro.* Biorheology, 1984. **21**(4): p. 617-30.

32. Davies, P.F., et al., *Turbulent fluid shear stress induces vascular endothelial cell turnover in vitro.* Proc Natl Acad Sci U S A, 1986. **83**(7): p. 2114-7.

33. DePaola, N., et al., *Vascular endothelium responds to fluid shear stress gradients.* Arterioscler Thromb, 1992. **12**(11): p. 1254-7.

34. Dewey, C.F., Jr., et al., *The dynamic response of vascular endothelial cells to fluid shear stress.* J Biomech Eng, 1981. **103**(3): p. 177-85.

35. Sprague, E.A., et al., *Flow-mediated modulation of selected biologic and molecular determinants related to vascular endothelial activation.* J Vasc Surg, 1992. **15**(5): p. 919-21.

36. Diamond, S.L., S.G. Eskin, and L.V. McIntire, *Fluid flow stimulates tissue plasminogen activator secretion by cultured human endothelial cells.* Science, 1989. **243**(4897): p. 1483-5.

37. Yoshizumi, M., et al., *Hemodynamic shear stress stimulates endothelin production by cultured endothelial cells.* Biochem Biophys Res Commun, 1989. **161**(2): p. 859-64.

38. Dull, R.O. and P.F. Davies, *Differential Endothelial Cytosolic Calcium Responses to Hemodynamic Shear Stress in vitro.* Circulation Suppl., 1989. **2**(481).

39. Berk, P., *Shear Stress Alters the Genetic Growth Program of Cultured Endothelial Cells.* Abstracts fo the First World Congress of Biomechanics, 1990. **2**(2): p. 315.

40. Ujiie, H., et al., *Effects of size and shape (aspect ratio) on the hemodynamics of saccular aneurysms: a possible index for surgical treatment of intracranial aneurysms.* Neurosurgery, 1999. **45**(1): p. 119-29; discussion 129-30.

41. Weir, B., et al., *The aspect ratio (dome/neck) of ruptured and unruptured aneurysms.* J Neurosurg, 2003. **99**(3): p. 447-51.

42. Investigators, I.S.o.U.I.A., *Unruptured intracranial aneurysms--risk of rupture and risks of surgical intervention. International Study of Unruptured Intracranial Aneurysms Investigators.* N Engl J Med, 1998. **339**(24): p. 1725-33.

43. LaMack, J.A. and M.H. Friedman, *Individual and combined effects of shear stress magnitude and spatial gradient on endothelial cell gene expression.* Am J Physiol Heart Circ Physiol, 2007. **293**(5): p. H2853-9.